Geochemistry, Geophysics, Geosystems

RESEARCH ARTICLE
10.1029/2018GC007852

Taphonomic and Ontogenetic Effects on Na/Ca and Mg/Ca in Spinose Planktonic Foraminifera From the Red Sea

E. M. Mezger[1], L. J. de Nooijer[1], M. Siccha[2], G.-J. A. Brummer[1,3], M. Kucera[2], and G.-J. Reichart[1,4]

[1]Royal Netherlands Institute for Sea Research, Department of Ocean System Sciences, and Utrecht University, Texel, Netherlands, [2]MARUM-Center for Marine Environmental Sciences, University of Bremen, Bremen, Germany, [3]Faculty of Earth and Life Sciences, Department of Earth Sciences, Cluster Earth and Climate, VU University Amsterdam, Amsterdam, Netherlands, [4]Faculty of Geosciences, Department of Earth Sciences, Utrecht University, Utrecht, Netherlands

Key Points:
- The chemical composition of Red Sea water-column planktonic foraminiferal shells from high salinity conditions was compared with specimens from the surface sediment
- Na/Ca ratios from core-top specimens are lower than those in water column specimens, whereas Mg/Ca is relatively high in the core-top specimens
- Specimens collected by plankton tows show decreasing Na/Ca with depth, probably associated with ongoing spine loss

Supporting Information:
- Supporting Information S1

Correspondence to:
E. M. Mezger,
eveline.mezger@nioz.nl

Citation:
Mezger, E. M., de Nooijer, L. J., Siccha, M., Brummer, G.-J. A., Kucera, M., & Reichart, G.-J. (2018). Taphonomic and ontogenetic effects on Na/Ca and Mg/Ca in spinose planktonic foraminifera from the Red Sea. *Geochemistry, Geophysics, Geosystems*, *19*, 4174–4194. https://doi.org/10.1029/2018GC007852

Received 24 JUL 2018
Accepted 28 SEP 2018
Accepted article online 13 OCT 2018
Published online 5 NOV 2018

Abstract As a recorder of the hydrological cycle and ocean circulation, salinity is one of the most wanted parameters in paleoceanography. Current paleosalinity reconstructions mostly rely on the interpretation of stable oxygen isotope signals combined with an independent paleotemperature proxy. Due to error propagation, this indirect approach is associated with large uncertainties. Recent culture studies and a Red Sea field study have shown that incorporation of Na in foraminiferal shell calcite depends on salinity, providing a potential direct proxy for salinity. However, application of a Na/Ca-based salinity proxy requires further calibration, which should also consider settling of foraminifera through the water column and burial in the sediment. Here we compare Na/Ca in living specimens from Red Sea surface waters with specimens collected from 0- to 500-m water depth and sedimentary specimens from core-tops. This shows that Na/Ca in *Globigerinoides ruber* and *Trilobatus sacculifer* shells decrease with increasing water depth and until the sediment surface. For both species, laser-ablation-ICP-Q-MS measurements combined with electron-probe microanalysis show that Na is enriched in the spines. Loss of spines during settling of foraminifera through the water column hence provides a mechanistic explanation for the observed Na decrease in bulk specimens with water depth. In contrast, average Mg/Ca values increase toward the seafloor in both species, coinciding with deposition of gametogenic calcite, which is enriched in Mg but has Na/Ca values similar to that in lamellar calcite. Both spine shedding and gametogenic calcite addition hence affect the average minor/trace element composition of foraminiferal calcite.

Plain Language Summary Investigating past climates (paleoclimatology) potentially provides valuable information of climatic functioning, which is essential in times of ongoing global warming. The amount of salts dissolved in seawater is an important factor when trying to reconstruct past ocean conditions. The distribution of salt—together with temperature—reflects ocean circulation, the balance between rainfall and evaporation (the hydrological cycle), and, on longer time scales, ice sheet formation or melting. Foraminifera, small organisms that produce shells consisting of calcite, record the conditions in which they grew by incorporating elements from the seawater in which they grew. For example, with more salts (e.g., sodium, Na) dissolved in seawater, foraminifera incorporate more Na their shells. Therefore, shell Na/Ca values can be used to reconstruct salinity. The accuracy of these reconstructions depends on the calibrations we have and also on the fundamental understanding involved in the preservation of the original Na/Ca ratio in shell carbonate. In this study, we found a difference in Na incorporation between foraminifera living in the surface water of the sea, floating with spines connected to the shell and shells recovered from the sediment. We describe the effect of the presence or absence of spines, high in Na, on total shell Na/Ca.

1. Introduction

Seawater salinity drives, together with temperature, the global thermohaline circulation, and therefore, it is a highly desired parameter in paleoceanographic reconstructions. Changes in salinity reflect important hydrological processes including river runoff, evaporation/precipitation and sea ice formation, and, on geological time scales, also the waxing and waning of continental ice sheets. Whereas many temperature proxies have been developed and are widely applied (e.g., $U^{k'}_{37}$ (Prahl & Wakeham, 1987), TEX86 (Schouten

et al., 2002), Mg/Ca (Elderfield & Ganssen, 2000; Lea et al., 1999; Nürnberg et al., 1996), and foraminiferal $\delta^{18}O$, for example (Zachos et al., 2001), proxies for past salinity remain, however, rather scarce (e.g., (Allen et al., 2016; Mezger et al., 2016; Rohling & Bigg, 1998; Schouten et al., 2006; Wit et al., 2013).

Paleosalinity reconstructions mostly involve combining independent (in-)organic temperature proxies with (foraminiferal) stable oxygen isotopes (Elderfield & Ganssen, 2000; Rohling & Bigg, 1998; Schouten et al., 2006; Vasiliev et al., 2017). Such an approach assumes a strong and constant relationship between salinity and stable isotopic composition of seawater. Since it is known that this relationship differs spatially (Zahn & Mix, 1991) and most probably also on geological time scales, a more sophisticated approach is required, involving modeling of the hydrosphere and its isotopes (Rohling & Bigg, 1998). Error propagation from calibrations and model assumptions on the hydrological regime result in relatively large uncertainties in reconstructed salinity (Rohling, 2007). These uncertainties can be circumvented by a more direct approach, that is, a salinity proxy that directly depends on elements defining seawater salinity (e.g., Na and Cl).

Salinity is defined as the total mass in grams of all dissolved substances in 1 kg of seawater. Although salinity varies because of differences in total amounts of dissolved salts, the relative contribution of the major constituents are constant. These elements, such as chloride, potassium, sulfur, and sodium, display a so-called conservative behavior. Most other elements do not show a one to one relation to salinity but vary as a consequence of many environmental parameters.

For most conservative elements, element incorporation does not vary with salinity, and a constant partitioning has been reported (De Nooijer et al., 2007; Evans et al., 2015; Hönisch et al., 2011; Lea & Boyle, 1991; Segev & Erez, 2006). However, for barnacle shells (Gordon et al., 1970), Atlantic oysters (Rucker & Valentine, 1961), and inorganic precipitates (Ishikawa & Ichikuni, 1984; Kitano et al., 1975), a correlation has been reported between salinity of the growth medium and carbonate bound Na/Ca. This implies that, although Na is a conservative element in seawater, its incorporation in calcium carbonate is not conservative. More recently, a significant positive relation between Na incorporation in foraminiferal shells and salinity was observed in culturing studies with benthic (Geerken et al., 2018; Wit et al., 2013) and planktonic foraminifera (Allen et al., 2016). A field study with living planktonic species (*Globigerinoides ruber* and *Trilobatus sacculifer*) from surface waters (plankton pump) collected from a transect spanning the largest part of the Red Sea (Mezger et al., 2016) confirmed the impact of salinity on foraminiferal Na incorporation, although absolute Na/Ca values are higher than those found in culturing studies. For applicability of a Na/Ca-based salinity proxy and to understand this offset between studies, further calibration studies are needed. Ideally, such studies should also take into account settling of foraminifera through the water column and their subsequent burial in the sediment.

To what extent primary signals are preserved in the sedimentary record is still unknown. Primary trace metal signals may be altered both during changes in habitat depth of living foraminifera in the water column (ontogenetic vertical migration) as well as during settling of the empty shells and upon burial in the sediment (taphonomic effects). These effects need to be quantified before such a potential proxy can be applied to sediment cores for paleoceanographic reconstructions. Therefore, we studied the alteration of the primary signal by comparing Na/Ca in specimens of *G. ruber* and *T. sacculifer* from surface waters with those collected by depth-stratified plankton tows to 500-m depth and from core-tops (0–1 cm) in the Red Sea. Comparing primary and potentially altered signals allows unraveling the influence of life stages as well as the export flux of postgametogenic (GAM) empty shells and early diagenesis from the impact on the shell chemical composition. Several processes, including the formation of GAM calcite (Nürnberg et al., 1996; Sadekov et al., 2005), crust formation (Steinhardt et al., 2015), inorganic overgrowths in high salinity environments (Hoogakker et al., 2009), or other diagenetic processes (e.g., etching due to partial dissolution [Brown & Elderfield, 1996] or Na leakage due to aging [Yoshimura et al., 2016]) might affect the original Na/Ca-salinity relationship. These ontogenetic (Nürnberg et al., 1996; Steinhardt et al., 2015) and diagenetic (Brown & Elderfield, 1996; Hoogakker et al., 2009) processes are known to influence the Mg/Ca composition of the shell, occasionally to such a degree that these can no longer be used for reliable temperature reconstructions. Because these processes impacting Mg/Ca are related to for instance a change in calcification strategy or early diagenesis, they could potentially also affect Na/Ca. To test this hypothesis, we perform electron-probe microanalyses (EPMA) of individual shells to investigate potential effects of ontogeny and depositional processes on the within-shell microdistribution of Mg and Na.

Table 1
Overview Cruises and Location of the Red Sea Core-top Samples[a]

Cruise	Name	Type	Lat [°N]	Long [°E]	Depth [m]	SSS	SST [^{0}C]
M 44/3	MC-601	MC	27.71	35.05	863	40.3	25.3
M 31/2	MC363	MC	25.52	35.61	941	40.0	25.8
M 31/2	MC364	MC	24.76	36.23	1185	39.8	26.7
M 5/2	MC-71	MC	23.39	36.98	1387	39.6	26.8
VA 29	707KG	BC	21.43	38.10	1985	39.1	28.0
M 5/2	MC-101	MC	20.11	38.42	2309	38.7	28.7
M 5/2	MC-107	MC	19.13	39.12	1161	38.3	29.1
M 31/2	MC366	MC	17.36	40.02	475	38.0	29.3
SO 121	SO-98	MC	15.94	41.68	959	37.3	29.0
SO 121	SO-100	MC	15.00	42.21	826	37.1	28.7
SO 121	SO-110	MC	12.25	44.47	740	36.3	28.0

[a]Sea surface salinities (SSS) and sea surface temperatures (SST) are retrieved from the WOA09_annual average. The gray bar coincides with the plankton tow location. MC: multicore, BC: box core.

2. Materials and Methods

2.1. Study Area and Sample Collection

For the present study, we sampled shells of planktonic foraminifera from sediments and the water column of the Red Sea to investigate the salinity dependency of foraminiferal Na/Ca along a strong natural salinity gradient. The Red Sea is characterized by a pronounced antiestuarine circulation (Rohling, 1994, and references therein), resulting in a strong south-north gradient in surface salinity. In contrast, annual mean temperature shows the opposite trend, with highest values in the middle to South. Red Sea and Gulf of Aden surface sediment samples were collected during three different cruises (for details see Siccha et al., 2009) from south to north (Table 1 and Figure 1).

After collection, core-top samples were washed over a 63-μm sieve, air dried and dry-sieved over a 150-μm mesh. The isolated specimens of *G. ruber* and *T. sacculifer* were cleaned according to the protocol described in Barker et al. (2003), with the exception of the reductive step. Foraminiferal diameters were determined by measuring the distance from the top of the final chamber (F) to the bottom between the F-1 and F-2 chamber. Based on their size, specimens were divided into four size categories corresponding to the mesh sizes used for the plankton tows (later this section). We targeted the symbiont-bearing planktonic foraminiferal species *G. ruber* and *T. sacculifer* as these species were most abundant and commonly used as proxy signal carriers globally. Average mean annual surface water temperature and salinity were taken from the world ocean atlas (WOA09: Antonov et al., 2010; Locarnini et al., 2010).

Depth-stratified plankton tows were taken using a modified Hydro Bios Multinet in May 2000 (RV *Pelagia* cruise 64PE158), covering the upper 10–500 m of the water column in eight discrete depth intervals at ~23.7°N and 36.8°E (which is close to core-top sample M5/2 MC-71, Figure 1 and Tables 1 and 2). Salinity and temperature profiles are based on the in situ measurement by a CTD cast deployed immediately prior to the Multinets (Table 2 and Figure 2). Upon collection, samples were drained on a 75-μm mesh sieve, shortly washed with ultrapure water to remove the salts, frozen, and stored at −40 °C. Sample processing was performed at the Royal Netherlands Institute for Sea Research (Royal NIOZ), located on the island of Texel, Netherlands. Samples were freeze dried, and a Low-Temperature-Asher was used to remove organic matter and thereby concentrate foraminiferal specimens (Fallet et al., 2009). A few drops of ethanol and ultrapure water were added to disperse the ashed residue, wet-sieved over a 63-μm mesh, and dried at 50 °C. According to Fallet et al. (2009), both methods (Barker protocol [Barker et al., 2003] and Low-Temperature-Asher) remove all organic material from foraminiferal shells and yield the same stable oxygen and carbon isotope and Mg/Ca values. To divide foraminiferal shells into several size categories, different mesh sizes were used for dry sieving (150, 250, 355, and 500 μm, respectively). Identification of species was performed using the ontogenetic species concept of (Brummer et al., 1987) for *Globigerinoides sacculifer* (Brady), later assigned to as *Trilobus sacculifer* (Spezzaferri et al., 2015), and *G. ruber* (d'Orbigny). Surface water (plankton pump) samples collected during the same cruise at the same location (respectively plankton pump 7) were described and analyzed in (Mezger et al., 2016).

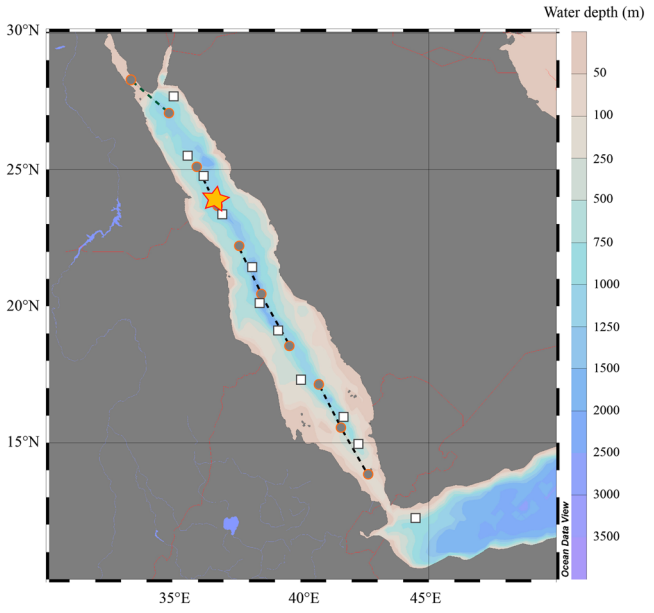

Figure 1. Map of sampling locations in the Red Sea. The star represents the location of plankton tows, the squares represent the core-top locations, and the surface water sample transects (published in Mezger et al., 2016) are indicated with the dots (start and end of transect) and dashed lines (transect).

2.2. LA-Q-ICP-MS Analyses

For the core-top samples, a total of 286 specimens with 37–11 specimens per location for *G. ruber* and 288 specimens with between 45 and 47 specimens per location for *T. sacculifer* were analyzed. For each plankton tow sample, at least 30 specimens were selected when available, measured,

Table 2
Position, Depth, Salinity, and Temperature During Plankton Tows, Derived From CTD Profiles (RV Pelagia cruise 64PE158)

Net	Lat [°N]	Long [°E]	Depth range [m]	Average salinity	Average temperature [^{0}C]
05c-net4	23.70	36.78	10–25	39.5	25.6
05c-net3	23.70	36.78	25–50	39.8	24.7
05c-net2	23.70	36.78	50–75	40.0	23.7
05c-net1	23.70	36.78	75–100	40.2	23.3
05a-net4	23.64	36.82	100–150	40.2	23.1
05a-net3	23.64	36.82	150–200	40.2	23.1
05a-net2	23.64	36.82	200–300	40.3	22.5
05a-net1	23.64	36.82	300–500	40.4	21.7

and grouped into one of four size classes to allow for testing the relation between size/life stage and element composition of the shells. In total, 238 specimens were measured for *G. ruber* and 133 specimens for *T. sacculifer*. Multiple measurements per specimens for subsequent chamber stages and duplicates on the same chamber were often performed and outliers removed by −2SD and +2SD.

After the cleaning, foraminifera were mounted on a stub with double-sided sticky tape with a nondetectable amount of the measured elements, ensuring that the tape does not affect the measurements. Laser ablation quadrupole inductively coupled plasma mass spectrometry (LA-Q-ICP-MS) was used to measure the elemental composition of the shells at the Royal NIOZ. The setup consisted of a NWR193UC (New Wave Research) laser, containing an ArF Excimer laser (ExciStar) with deep UV 193-nm wavelength and <4-ns pulse duration, coupled to a quadrupole ICP-MS (iCAP-Q, Thermo Fisher Scientific). Due to different ablation thresholds, laser ablation for calcite was performed with a fluence of 1 J/cm^2 at a repetition rate of 6 Hz, while the glass NIST-610 and NIST-612 standards were ablated with a fluence of 5 J/m^2. This difference in fluence was found previously not to influence results for Mg and Sr (Dueñas-Bohórquez et al., 2011; Hathorne et al., 2008).

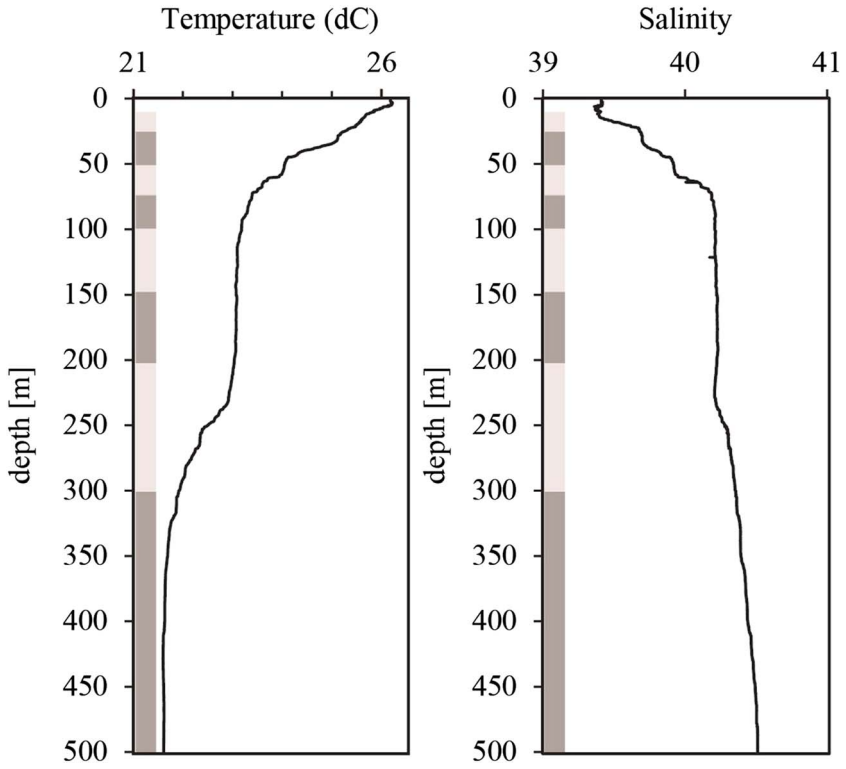

Figure 2. In situ depth profiles of the water column at the site where the plankton tow samples were collected. Depth intervals of the plankton tows are indicated at the left side of the graphs.

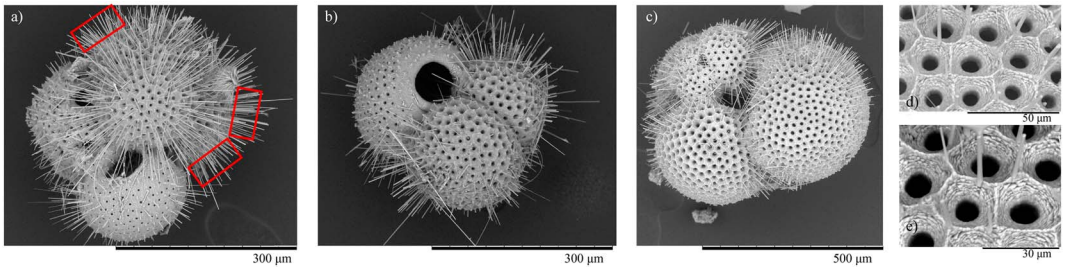

Figure 3. Scanning electron microscopy pictures of foraminifera from plankton tow 05c-net4, with (a and b) *G. ruber* with spines and examples of LA-spots and (c) *T. sacculifer* with spines (and zoomed-in, d and e).

Specimens were ablated between 40 to 60 s, depending on the thickness of the wall and size of the chamber. Using a dual-volume cell, helium was used as a carrier gas with a flow rate of 0.5 L/min, which is mixed between the ablation cell and mass spectrometer with Argon (Ar) makeup gas and 0.003 mL/min N_2. The Ar makeup gas was adjusted using the normalized Ar index (Fietzke & Frische, 2016). Torch position, collision cell technology focus and extraction lens were optimized daily. The ThO/Th ratio, a measure for oxide formation, was always $<$0.5%. The masses monitored by the ICP-MS were ^{7}Li, ^{11}B, ^{23}Na, ^{24}Mg, ^{25}Mg, ^{27}Al, ^{43}Ca, ^{44}Ca, ^{57}Fe, ^{88}Sr, ^{138}Ba, and ^{238}U, with a duration of 0.12 s for one cycle through these 12 masses. In between the laser and ICP-MS, a smoother is used optimizing the signal. Every run started and ended with a 20-s gas blank. A spot size of 80 µm was used to ablate the shells. Elemental ratios of the shells and standards were calibrated and calculated following the method described in van Dijk et al. (2017). The calcium carbonate standard MACS-3 (Wilson et al., 2008) was used for a linear correction for potential drift during each run and therefore ablated after every 10 samples. Relative analytical precision (in RSD) of all MACS-3 measurements is 3.9% for ^{23}Na, 3.3% for ^{24}Mg, and 3.1% for ^{25}Mg, with accuracies of 100.2% for Na/Ca (based on ^{23}Na) and 100.1% for Mg/Ca (averaged ^{24}Mg and ^{25}Mg) compared to the reference values. Results from our in-house foraminiferal standard (NFHS-1; Mezger et al., 2016) indicated a relative analytical precision of 5.8% for ^{23}Na, 11.3% for ^{24}Mg, and 11.6% for ^{25}Mg, with accuracies of 96.7% for Na/Ca and 90.3% for Mg/Ca. At the start and end of each measurement series, the glass NIST-610 and NIST-612 standards were measured and compared to elemental values reported earlier (Jochum et al., 2011). For NIST-610, a relative precision of 4.4% for ^{23}Na, 4.6% for ^{24}Mg, and 3.9% for ^{25}Mg was observed, with accuracies of 106.7% for Na/Ca and 110% for Mg/Ca compared to reference values. For NIST-612, a precision of 3.5% for ^{23}Na, 2.9% for ^{24}Mg, and 3.2% for ^{25}Mg was observed, with accuracies of 107.8% for Na/Ca and 94% for Mg/Ca compared to reference values.

For LA-Q-ICP-MS of the foraminiferal spines, settings used were similar to the shell carbonate analyses, but with a rectangular (40 $\times$ 80 µm) shaped "spot" and a delay of only 1 s after switching on the laser. In total, 31 measurements on foraminiferal spines of both *G. ruber* and *T. sacculifer* were performed, focusing on clusters of spines outside of different shells (example measured specimens: Figure 3). Aliasing was avoided by using very short cycle times, with every cycle, measuring ^{23}Na, ^{24}Mg, and ^{43}Ca, costing only 0.03 s, whereas the laser ablated every 0.17 s (6 Hz).

For some ablations Mg was excluded from the analytical matrix (in which case a cycle lasted only 0.02 s), as we used the first series of analyses to test our setup for Na/Ca only. Due to the low quantity of calcium carbonate when ablating spines, laser ablation profiles were relatively short. Using only the data with at least a modest Ca signal, data acquisition lasted between 2 and 16 s for the individual analyses (Tables 5 and 6). Such short profiles are generally disregarded (e.g., Mezger et al., 2016), however, for our purposes and due to the very short cycle times used, still suitable. During spine measurements, for MACS-3, a relative precision of 8.88% is observed for Na/Ca based on ^{23}Na and 6.76% for ^{24}Mg, with accuracies of 100.6% and 99.97% compared to reference values.

2.3. Electron Probe Micro Analyses and Scanning Electron Microscopy

Surface structures of the laser-ablated foraminifera were studied using scanning electron microscopy (SEM3000, Hitachi). For this, magnifications between 150 and 2.5 * 10^3 were used.

Directly upon low-temperature ashing, multinet specimens (RV *Pelagia* cruise 64PE158) were isolated for spine analysis and transferred without sieving to preserve the spines. After addition of ethanol and a few

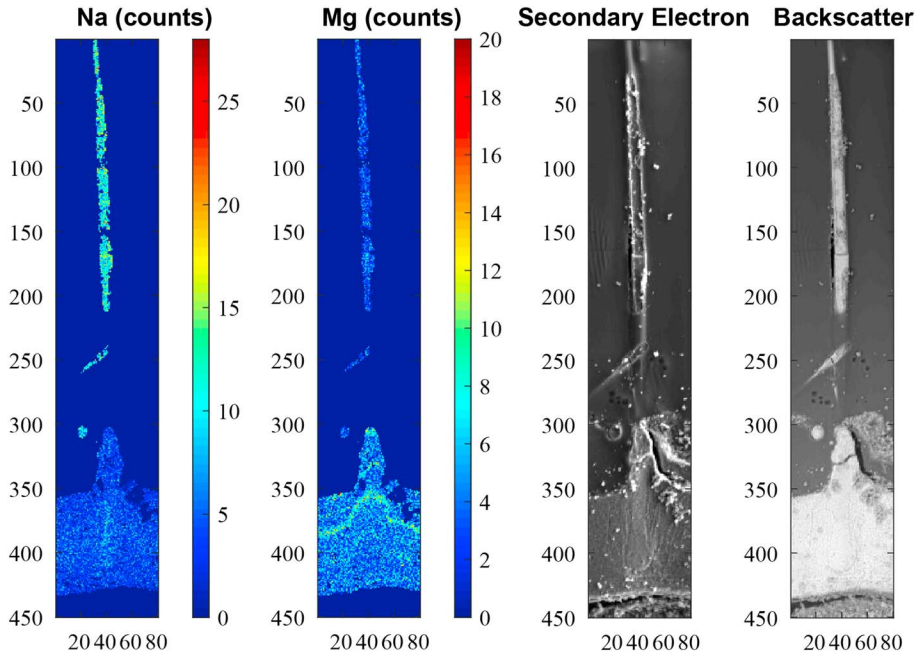

Figure 4. Example of the identification of a (in this case) *T. sacculifer* spine still attached to the shell by secondary electron and backscatter electron imaging, with its corresponding electron probe micro analysis Na (counts) and Mg (counts) map. The number of pixels (1 pixel: 0.2 μm) is indicated at the left side and bottom of the images.

drops of ultrapure water, to disaggregate the sample, a saturated $CaCO_3$ solution was added to avoid any dissolution of spines. *G. ruber* and *T. sacculifer* specimens were transferred with a glass pipette into a clean Petri dish, in which they were rinsed with ultrapure water three times. Multiple specimens with abundant spines (which were most specimens isolated this way) were embedded in resin (Araldite 20/20) in a vacuum chamber to avoid air bubbles being trapped in the samples. After 48 hr in an oven at approximately 50 °C, the resin was fully hardened and specimens were polished and carbon coated.

Whole shell and spine element mapping for Na, Mg, and Ca was performed with an electron microprobe at Utrecht University (JEOL JXA-8530F Field emission Electron Probe Micro Analyzer). Maps were generated with a focused electron beam with a beam current of 10 nA and an accelerating voltage of 7 kV. The dwell time was set at 300 ms and a step/pixel size of 0.2 μm (Figure 4). Counts, representing current strength, were converted to elemental ratios using analyses on standard material. We used Jadeite for Na, foraminiferal calcite for Ca, and Forsterite for Mg, assuming a linear dependency of concentration (in mass %) on the signal and a constant background. Background intensities, measured for the same (foraminiferal) samples with similar settings as the measurements, were first subtracted from the total element intensities before converting to mass %. Pixel-based quantifications were eliminated from further analyses when the Ca mass percentage was below 30%. Identification of spines and spine-related structures was based on backscatter and secondary electron imaging (Figure 4).

3. Results

3.1. Depth-Stratified Plankton Tows

3.1.1. Na/Ca

For *G. ruber*, average Na/Ca values from the plankton tows (per depth interval) vary between 10.30 ± 0.24 and 6.93 ± 0.05 mmol/mol, and for *T. sacculifer* between 9.28 ± 0.11 and 6.69 ± 0.11 mmol/mol (Table 3 and Figure 5). Very few specimens of *T. sacculifer* were found at depths between 200 to 500 m, thereby limiting observations of Na/Ca change at larger depth. Still, for both species, a significant negative trend is observed between Na/Ca and depth (m) (Na/Ca = −0.027 * depth [m] + 9.14, $r^2 = 0.53$ and $p < 0.001$ for *G. ruber* and Na/Ca = −0.032*depth [m] + 9.93, $r^2 = 0.77$ and $p < 0.001$ for *T. sacculifer*) in the upper 100 m of the water column, when combined with surface water plankton samples (Mezger et al., 2016; Figure 5). This trend

Table 3
*Overview of Sampling Depth and Elemental Ratios (*mmol/mol) of Specimens From Red Sea Plankton Tows, With n = Number of Specimens, nm = Number of Measurements Performed, Including Duplicates of Specimens Excluding Outliers*[a]

Net	Depth range [m]	Species	n	nm	Na/Ca*	SD	SE	nm	Mg/Ca*	SD	SE	Avg S	Avg T
05c-net4	10–25	*G. ruber*	30	52	10.3	1.74	0.24	54	4.65	0.87	0.12	39.5	25.6
		T. sacculifer	30	61	9.28	0.86	0.11	62	4.58	0.90	0.11		
05c-net3	25–50	*G. ruber*	34	65	8.22	0.63	0.08	65	6.38	0.89	0.11	39.8	24.7
		T. sacculifer	30	40	8.06	0.93	0.15	40	3.92	0.62	0.10		
05c-net2	50–75	*G. ruber*	34	62	7.16	0.61	0.08	65	5.68	1.19	0.15	40.0	23.7
		T. sacculifer	30	82	8.44	0.82	0.09	86	5.00	1.11	0.12		
05c-net1	75–100	*G. ruber*	30	54	8.08	0.42	0.06	56	6.85	1.17	0.16	40.2	23.3
		T. sacculifer	20	33	6.69	0.66	0.11	33	4.95	1.41	0.24		
05a-net4	100–150	*G. ruber*	25	46	6.93	0.35	0.05	46	6.43	1.02	0.15	40.2	23.1
		T. sacculifer	4	13	7.11	0.52	0.14	14	6.62	1.18	0.32		
05a-net3	150–200	*G. ruber*	30	78	7.48	0.68	0.08	76	6.85	1.34	0.15	40.2	23.1
		T. sacculifer	16	62	9.12	1.10	0.14	62	4.54	1.00	0.13		
05a-net2	200–300	*G. ruber*	25	62	7.94	0.71	0.09	62	5.86	1.19	0.15	40.3	22.5
		T. sacculifer	1	-	-	-	-	-	-	-	-		
05a-net1	300–500	*G. ruber*	30	48	7.17	0.49	0.07	49	5.92	1.17	0.17	40.4	21.7
		T. sacculifer	2	3	7.46	0.74	0.43	3	4.74	0.22	0.12		

[a]Salinity (S) and temperatures (T) are derived from CTD profiles during RV Pelagia cruise 64PE158, n:n^{o} specimens.

reverses below 100 m, as Na/Ca in both species increases slightly from 100 to 200 m depth (Figure 5). In general, lower Na/Ca values are observed for larger sized foraminiferal shells of *T. sacculifer* (Figure S1 and Tables S2 and S3 in the supporting information). For *G. ruber* no clear trend is observed with shell size within the water column, albeit that Na/Ca values of size class 2 (250–355 μm) lower than or similar to size class 1 (150–250 μm; Figure S1). For further details on shell size and relative distributions, see supporting information 1.1.

3.1.2. Mg/Ca

Average Mg/Ca values per depth interval for *G. ruber* vary between 4.65 ± 0.16 and 6.85 ± 0.12 mmol/mol, and for *T. sacculifer* between 3.92 ± 0.10 and 6.62 ± 0.32 mmol/mol (Table 3), with almost consistently higher Mg/Ca for *G. ruber* compared to *T. sacculifer*. From 0- to 150-m depth (including surface water specimens), Mg/Ca values for both species increase significantly with water depth (*G. ruber*: $y = 0.013x + 5.5$, $r^2 = 0.50$, $p < 0.001$, *T. sacculifer*: $y = 0.016x + 3.94$, $r^2 = 0.64$, $p < 0.001$). In the upper 150 m, average Mg/Ca values decrease again and subsequently remain similar with increasing water depth. No clear trend of Mg/Ca with size is observed for *G. ruber* nor *T. sacculifer* from the plankton tows, even though in some depth intervals, differences between size classes are observed (Figure S2 and Tables S4 and S5).

3.2. Core-Tops

3.2.1. Na/Ca

The final chamber (F), F-1, and F-2 were measured where possible, depending on size and preservation, while avoiding the sac-chamber for *T. sacculifer*. Average Na/Ca values per core-top location vary from 6.34 (±0.07) mmol/mol to 8.00 (±0.22) mmol/mol for *G. ruber* and between 5.36 (±0.04) and 6.76 (±0.07) for *T. sacculifer* (Table 4). For *G. ruber*, relative standard deviations are between 5 and 9.9% per location, whereas the RSEs are much smaller (between 0.8 and 1.3%) because of the relatively large number of measurements performed (Table 4). For *T. sacculifer*, relative standard deviations are between 7 and 13.2% percent per location, whereas the RSEs are between 0.5 and 2.1% (Table 4).

With salinity (WOA09: Antonov et al., 2010; Locarnini et al., 2010), *T. sacculifer* Na/Ca shows a significant correlation ($y = 0.14x + 0.41$, $R^2 = 0.15$, $p < 0.0001$), whereas for *G. ruber*, salinity and Na/Ca are not correlated ($y = 0.005x + 6.52$, $R^2 = 0.0004$, $p = 0.8$; Figure 6). Shell size does not have a significant effect on the Na/Ca ratio with depth for either species (for further details: supporting information 2.1).

3.2.2. Mg/Ca

For *G. ruber* and *T. sacculifer* (Figure 6), Mg/Ca changes significantly with SST from north to south along the investigated transect ($p < 0.001$ for both species, $y = -0.41x + 19.03$ and $r^2 = 0.16$ for *G. ruber*, $y = -0.62x + 23.46$, $r^2 = 0.58$ for weighted averaged *T. sacculifer*). Highest values are observed in the

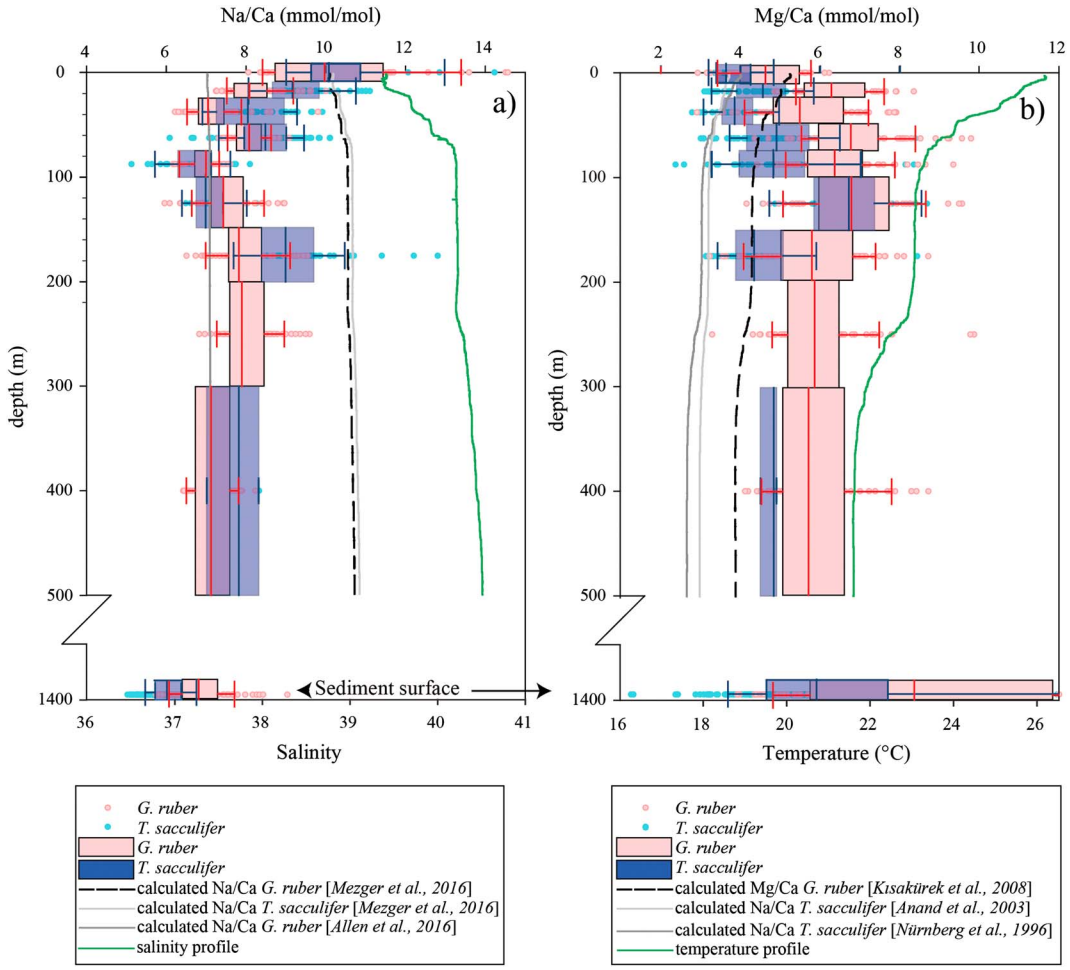

Figure 5. Plankton tows (a) Na/Ca and (b) Mg/Ca box-whisker plots, indicating median, first and third quartiles, and maxima and minima. The dots that fall outside this plot indicate individual single-chamber Na/Ca and Mg/Ca. For clarity, the highest Mg/Ca values of the sediment surface fall partly outside the plotted range (Table 4 and Figure 6). For comparison, examples of expected Na/Ca and Mg/Ca values are also indicated, based on salinity and temperature depth profiles and existing Na/Ca-salinity calibrations (Allen et al., 2016; Mezger et al., 2016), Mg/Ca-temperature calibrations (Anand et al., 2003; Nürnberg et al., 1996), and an Mg/Ca-temperature and salinity calibration (Kısakürek et al., 2008).

northern part of the transect, which is characterized by the lowest temperatures and highest salinities. A slight significant positive correlation between shell size and Mg/Ca is observed for *T. sacculifer,* albeit that r^2 is very low (supporting information: $y = 5.6x + 636.9$, $r^2 = 0.013$, $p = 0.001$). This is in line with the high variability observed in the data (Figure S4 and supporting information 2.2). For *T. sacculifer*, highest Mg/Ca values are found in specimens larger than 500 μm in size, a size class that was not observed in the water column plankton samples.

3.3. Spines

3.3.1. Laser Ablation

Since spine laser ablation profiles are relatively short, outliers potentially have a major effect on average element/Ca (El/Ca) ratios. Therefore, raw data were first evaluated and ^{43}Ca intensities below 6,000 counts per second (with an average ^{43}Ca background of approximately 1,000 counts per second) were eliminated from further calculations. Subsequently, averages were calculated based on two different approaches: First the molar ratio was calculated using the integrated profile (i.e., the average of the El/Ca ratios throughout the profiles) and second by averaging single scan ratios. The last approach allows distinguishing mean (average Na/average Ca) and median for all spine measurements per species combined (Figure 7). Calculating the median minimizes the effect of tailing or outliers compared to the mean. When combining Na/Ca ratios from

Table 4
*Overview Measured Elemental Ratios (*mmol/mol) Red Sea Core-top Samples, With n = Number of Specimens, nm = Number of Measurements Performed, Including Duplicates of Specimens Excluding Outliers*[a]

Cruise	Name	Species	n	nm	Na/Ca*	SD	SE	nm	Mg/Ca*	SD	SE	SSS	SST[^{0}C]
M 44/3	MC-601	*G. ruber*	31	58	6.64	0.45	0.06	59	7.70	2.16	0.28	40.3	25.3
		T. sacculifer	37	64	5.86	0.65	0.08	63	6.47	2.71	0.34		
M 31/2	MC363	*G. ruber*	11	12	8.02	0.75	0.22	12	9.77	3.15	0.91	40.0	25.8
		T. sacculifer	38	69	6.76	0.60	0.07	68	7.47	3.39	0.41		
M 31/2	MC364	*G. ruber*	30	62	6.39	0.39	0.05	63	9.35	3.22	0.41	39.8	26.7
		T. sacculifer	30	62	5.72	0.76	0.10	60	6.86	3.29	0.42		
M 5/2	MC-71	*G. ruber*	22	76	6.89	0.68	0.08	76	9.29	4.17	0.48	39.6	26.8
		T. sacculifer	36	242	6.08	0.49	0.03	242	7.44	4.67	0.30		
VA 29	707KG	*G. ruber*	30	59	6.37	0.42	0.05	57	6.09	1.32	0.17	39.1	28.0
		T. sacculifer	28	154	5.79	0.41	0.03	156	5.31	1.40	0.11		
M 5/2	MC-101	*G. ruber*	37	55	6.93	0.53	0.07	53	8.25	2.39	0.33	38.7	28.7
		T. sacculifer	45	93	6.05	0.55	0.06	93	5.66	2.19	0.23		
M 5/2	MC-107	*G. ruber*	30	28	6.86	0.48	0.09	30	8.02	2.18	0.40	38.3	29.1
		T. sacculifer	16	41	6.02	0.43	0.07	41	6.09	2.22	0.35		
M 31/2	MC366	*G. ruber*	30	53	6.63	0.50	0.07	54	7.15	1.92	0.26	38.0	29.3
		T. sacculifer	32	113	5.36	0.46	0.04	111	4.79	1.37	0.13		
SO 121	SO-98	*G. ruber*	20	43	7.02	0.35	0.05	43	7.72	1.65	0.25	37.3	29.0
		T. sacculifer	12	42	6.17	0.67	0.10	42	5.37	2.25	0.35		
SO 121	SO-100	*G. ruber*	17	39	7.01	0.34	0.05	40	6.67	1.66	0.26	37.1	28.7
		T. sacculifer	7	22	5.98	0.59	0.13	22	6.67	1.79	0.38		
SO 121	SO-110	*G. ruber*	28	47	6.34	0.49	0.07	46	5.01	1.17	0.17	36.3	28.0
		T. sacculifer	7	14	5.82	0.63	0.17	12	4.10	0.98	0.28		

[a]Sea surface salinities (SSS) and sea surface temperatures (SST) are retrieved from the WOA09_annual average.

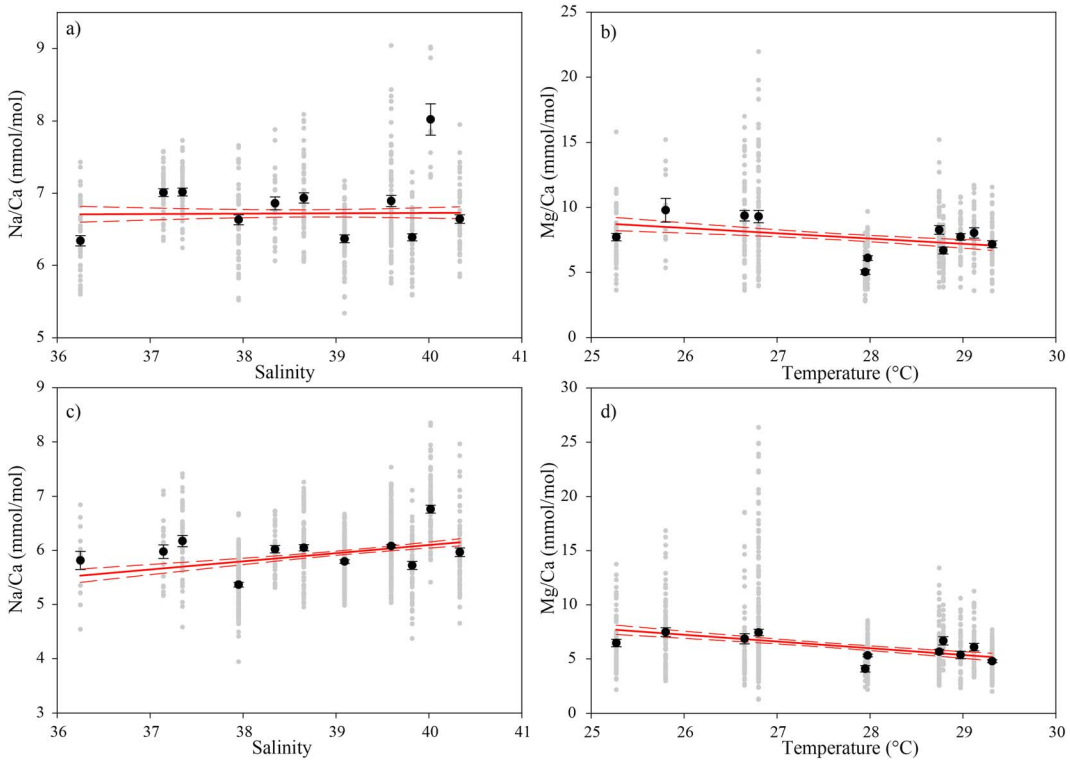

Figure 6. (a and c) Core-top Na/Ca and (b and d) Mg/Ca values, plotted against SSS (Na, WOA09) and latitude (Mg, WOA09) with (a) *G. ruber* Na/Ca, averages, and SE are indicated, as well as the linear regression and 95% confidence interval; (b) *G. ruber* Mg/Ca; (c) *T. sacculifer* Na/Ca; (d) *T. sacculifer* Mg/Ca.

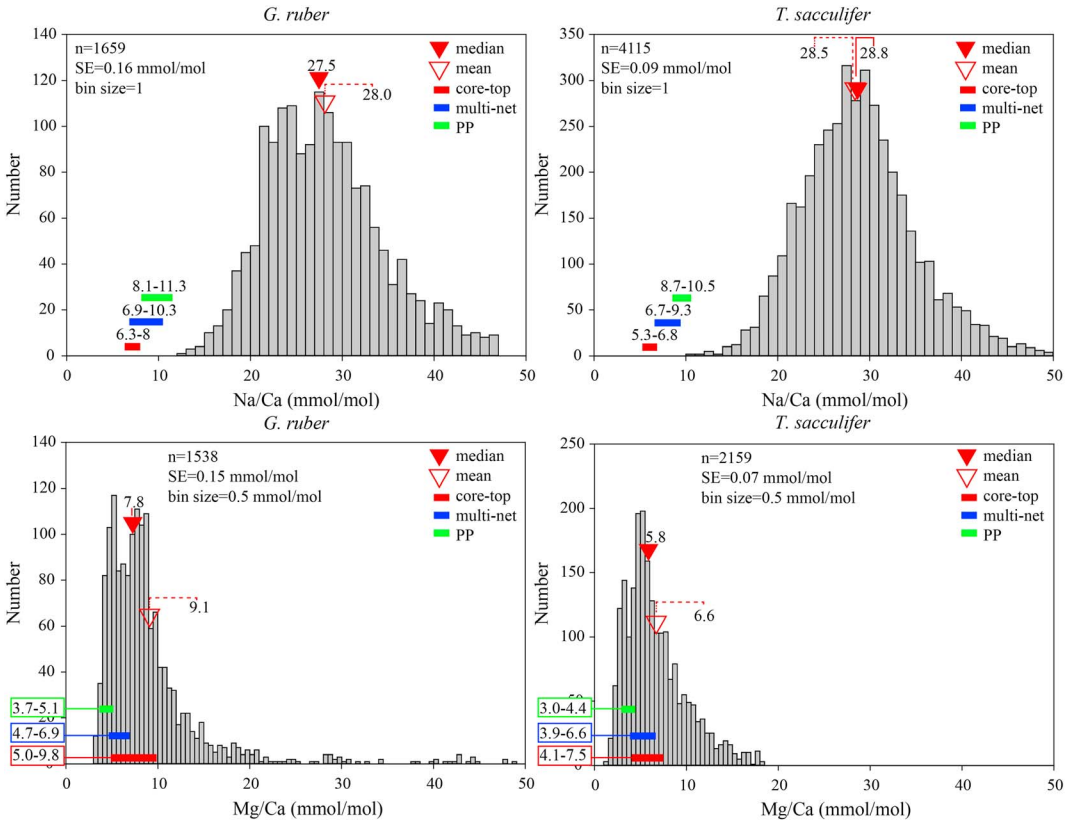

Figure 7. Spine distribution plots for all Na/Ca and Mg/Ca (mmol/mol) measurements for *G. ruber* and *T. sacculifer*, including average Na/Ca and Mg/Ca ranges (entire Red Sea) for specimens from core-tops, plankton tows (multinet), and plankton pump (PP) specimens.

all individual scans (Figure 7), average *G. ruber* spine Na/Ca values vary from 27.5 (median) to 28.0 mmol/mol (mean), and average Na/Ca values for *T. sacculifer* spines vary from 28.5 (mean) to 28.8 mmol/mol (median; Figure 7). For Mg/Ca, average *G. ruber* spine values vary from 7.8 (median) to 9.1 mmol/mol (mean), whereas *T. sacculifer* spine values vary from 5.8 (median) to 6.6 (mean). Because the ablations of the spines were more or less of similar duration, the data from the individual scans (average of individual scans) and from combined ablations (combining raw data from all measurements) compare well. Average spine Na/Ca and Mg/Ca (mmol/mol) values of the separate measurements are hence similar to the average of the combined raw data (Tables 5 and 6 and Figure 7). For *G. ruber*, average spine Na/Ca values from separate profiles (Table 5) vary from 26.7 (median) to 27.4 mmol/mol (mean), while for *T. sacculifer* averages vary from 29.3 (median) to 30.6 mmol/mol (mean; Table 6). Values for Mg/Ca vary on average from 7.4 (median) to 11.0 (mean) for *G. ruber* and from 5.1 (median) to 6.9 (mean) for *T. sacculifer* (Tables 5 and 6). The standard deviation per ablation is less than the average standard deviation for the grouped analyses (Tables 5 and 6).

3.3.2. EPMA

For both species, EPMAs show that Na is not homogeneously distributed within the shell wall (Figures 4, 8, and 9). However, unlike Mg, the distribution of Na does not show clear banding, but a more patchy distribution with clear zones of higher concentrations in the spine region. Measurements on spines of both species show Na/Ca values similar to those established by LA-ICP-MS (section 3.3.1), which are much higher than the average shell Na/Ca values (Figures 4, 8, and 9). However, it was more challenging to measure *G. ruber* spines than *T. sacculifer* spines, as these were much thinner and more easily lost in the polishing process. Spine Mg/Ca values are similar to or lower than shell Mg/Ca values (Figures 7 and 4), based on both LA-ICP-MS and EPMAs.

Table 5
Overview of Spine Measurements With Elemental Ratios in mmol/mol, With s: Duration Spine Integration Interval (s) and n: number of Measurements During s

Net	Depth range (m)	Species	Mean						Median			
			s	n (~)	Na/Ca	±	Mg/Ca	±	Na/Ca	±	Mg/Ca	±
net 4	10_25	*G. ruber*	14	538	34.1	1.6	17.8	0.9	32.1	1.5	9.2	0.4
net 4	10_25	*G. ruber*	2	77	27.7	0.8	7.7	0.2	27.3	0.8	7.1	0.2
net 4	10_25	*G. ruber*	4	121	28.8	1.1			27.7	1.1		
net 4	10_25	*G. ruber*	4	154	23.7	1.0	8.9	0.4	23.2	0.9	7.4	0.3
net 4	10_25	*G. ruber*	9	346	22.3	0.7	5.9	0.2	21.9	0.7	5.2	0.2
net 4	10_25	*G. ruber*	10	385	37.3	1.5	14.5	0.6	35.4	1.5	9.5	0.4
net 4	10_25	*G. ruber*	5	192	27.2	1.3	5.3	0.3	27.2	1.3	4.9	0.2
net 4	10_25	*G. ruber*	2	77	26.7	1.1	7.6	0.3	25.9	1.1	5.6	0.2
net 4	10_25	*G. ruber*	4	154	20.3	0.8	14.4	0.6	19.9	0.8	9.6	0.4
net 4	10_25	*G. ruber*	3	115	26.4	1.1	17.2	0.7	26.4	1.1	8.6	0.4
Total number of measurements				2,159								
Average (mmol/mol)					27.4		11.0		26.7		7.4	
(Average) SD					5.1	1.1	4.9	0.5	4.6	1.1	1.9	0.3
(Average) SE					1.6		1.6		1.5		0.6	

3.4. Shell Wall Surface Structure

Scanning electron microscopy pictures reveal that the shells of specimens collected from core-tops differ from those of the same species collected from the water column (~17.5 m, Figure 4) in terms of wall thickness, average test size (within the plankton pump samples specimens never reached the size observed in the core-tops), and surface texture (Figures 4, 10, and 11). In general, surface water specimens are smaller (~125–500 μm for *T. sacculifer* and ~125–350 μm for *G. ruber*), have spines, and are thin-walled. The outer surface of the final chamber is often smoother than the other chambers, particularly for preadult or young adult specimens (Brummer et al., 1987). Coarse surface textures with spines growing from or near the corners are

Table 6
Overview of Spine Measurements With Elemental Ratios in mmol/mol, With s: Duration Spine Integration Interval (s) and n: number of Measurements During s

Net	Depth range (m)	Species	Mean						Median			
			s	n (~)	Na/Ca	±	Mg/Ca	±	Na/Ca	±	Mg/Ca	±
net 4	10_25	*T. sacculifer*	5	130	32.0	4.9	7.3	0.3	31.7	4.8	4.0	0.2
net 4	10_25	*T. sacculifer*	5	130	28.7	3.5	8.2	0.5	28.5	3.5	5.9	0.3
net 4	10_25	*T. sacculifer*	3	78	26.9	3.5	6.4	0.2	26.8	3.5	3.8	0.1
net 4	10_25	*T. sacculifer*	10	261	23.7	1.7	5.8	0.3	23.5	1.7	5.2	0.2
net 4	10_25	*T. sacculifer*	7	183	23.0	2.0	4.2	0.2	22.9	2.0	3.3	0.1
net 4	10_25	*T. sacculifer*	5	130	19.1	2.2	4.9	0.2	18.9	2.2	3.5	0.2
net 4	10_25	*T. sacculifer*	8	209	32.2	3.5	7.6	0.3	31.2	3.4	6.2	0.3
net 4	10_25	*T. sacculifer*	3	78	29.2	5.2	6.9	0.3	28.8	5.2	3.1	0.1
net 4	10_25	*T. sacculifer*	13	339	33.7	3.2	7.6	0.4	32.6	3.1	6.2	0.3
net 4	10_25	*T. sacculifer*	16	417	28.9	2.5	10.4	0.5	29.1	2.5	9.4	0.5
net 4	10_25	*T. sacculifer*	2	98	33.7	1.0			32.4	1.0		
net 4	10_25	*T. sacculifer*	6	294	34.1	1.1			29.3	0.9		
net 4	10_25	*T. sacculifer*	5	245	29.0	1.0			28.4	1.0		
net 4	10_25	*T. sacculifer*	6	294	27.3	0.9			27.2	0.9		
net 4	10_25	*T. sacculifer*	6	294	27.1	0.9			26.6	0.9		
net 4	10_25	*T. sacculifer*	7	343	27.6	0.9			27.2	0.9		
net 4	10_25	*T. sacculifer*	2	98	48.7	2.0			37.0	1.6		
net 4	10_25	*T. sacculifer*	2	98	41.5	1.0			39.9	1.0		
net 4	10_25	*T. sacculifer*	5	245	34.2	0.9			32.3	0.9		
net 4	10_25	*T. sacculifer*	3	147	31.8	0.7			31.1	0.7		
total number of measurements				4,115								
average (mmol/mol)					30.6		6.9		29.3		5.1	
(average) SD					6.5	2.1	1.8	0.3	4.7	2.1	1.9	0.2
(average) SE					1.4		0.6		1.1		0.6	

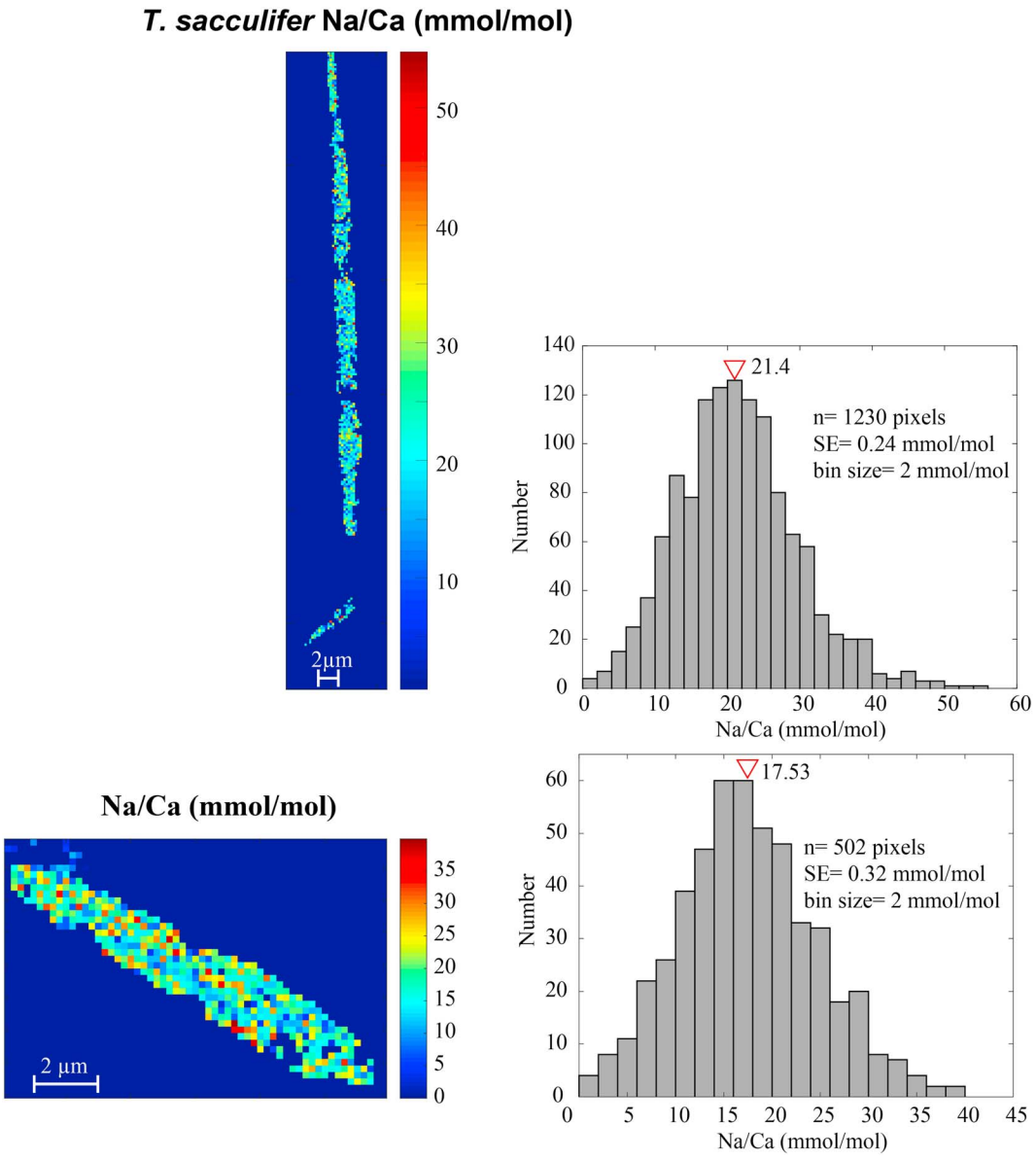

Figure 8. *T. sacculifer* electron-probe microanalysis spine measurements and accompanying histograms.

commonly observed in living *T. sacculifer* but are less pronounced in *G. ruber* (Figures 4 and 10). Such topography arising from the spine-shell interface is usually more pronounced in larger specimens, where the buildup of calcite plaques around the spine bases (Bé, 1980; Hemleben, 1975) results in terraced structures. Unfortunately, spines partially broke off in specimens collected from surface water due to the plankton pump sampling and sample processing. In the depth-stratified plankton tows (~17.5 m depth, Figure 4), specimens have thicker and longer spines and shell walls appear also somewhat thicker compared to those from surface waters. The former also show a better developed cancellate surface texture in *T. sacculifer,* as well as a thicker buildup of calcite plaques around the base of the spines in *G. ruber*.

Compared to specimens collected from the water column, those from core-tops are larger (184–516 µm for *G. ruber* and 229–1,284 µm for *T. sacculifer*), do not have spines, and have much thicker shell walls, which also appears to be reflected in generally longer laser ablation profiles. Both species show surface textures with indications for processes preceding gamete release, for example, "smoother" surfaces caused by deposition of GAM calcite, spine holes, thicker shell walls, and terminal ontogenetic features like the sac-like chamber in *T. sacculifer* (Bé, 1980; Bijma & Hemleben, 1994; Brummer et al., 1987; Figure 11). Often, specimens with

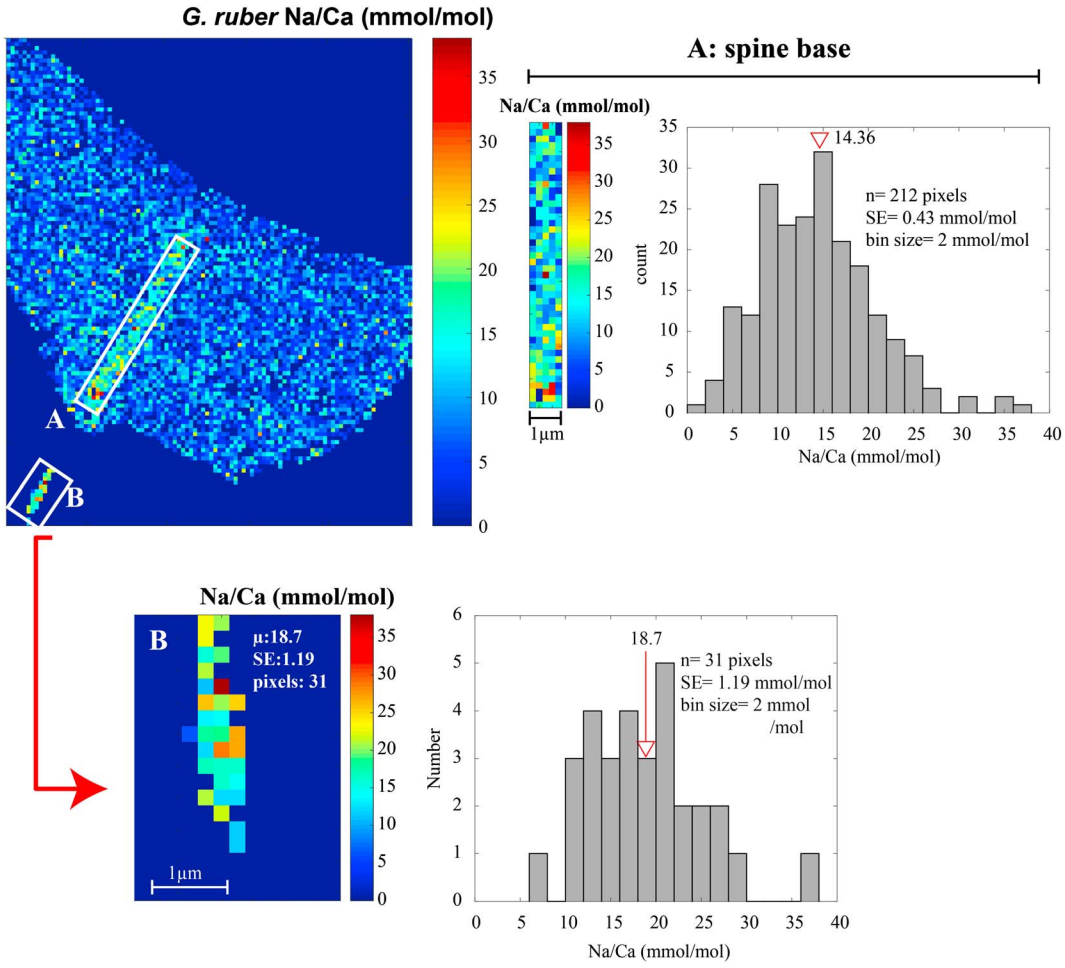

Figure 9. *G. ruber* electron-probe microanalysis spine measurements and accompanying histograms.

(abnormally) high Mg/Ca values in the northernmost part of the Red Sea also display signs of dissolution of the shell's surface in combination with a thick shell wall that no longer displays clear ridges and/or hexagonal patterns (Figure 11). The high-Mg phase of these specimens is often visible in the laser ablation profiles as elevated Mg/Ca at the outer surface (Figure 11), while inorganic overgrowth crystals appear absent. Depending on the thickness and absolute Mg/Ca of this layer, the average Mg/Ca may be elevated.

4. Discussion

Average shell Na/Ca values of *G. ruber* and *T. sacculifer* collected from Red Sea core-tops (Figure 12) correspond well to values reported in previous culture and field studies of the same species (Allen et al., 2016; Delaney et al., 1985) and to those of cultured benthic foraminifer *Ammonia tepida* (Wit et al., 2013) but are significantly lower than those of the same species collected from surface waters of the Red Sea (Mezger et al., 2016). In addition, the correlation between Na/Ca and salinity of surface water planktonic species collected in situ (Mezger et al., 2016) is absent in the specimens from the core-tops.

In the southern Red Sea Mg/Ca values are similar to those reported earlier (Allen et al., 2016; Anand et al., 2003; Kısakürek et al., 2008), but in the northern Red Sea, we find values higher compared to earlier work (Allen et al., 2016; Anand et al., 2003; Kısakürek et al., 2008) and also higher than in the same species collected from surface waters of the Red Sea (Mezger et al., 2016). Mg/Ca values in the northern Red Sea are too high to be explained by known temperature and salinity dependencies and reach values comparable to those from earlier Mediterranean studies (Ferguson et al., 2008), a sea which is also a known for its overall high salinity. Still, other studies in the Mediterranean looking at Mg/Ca values suggest calibrations rather similar to that for

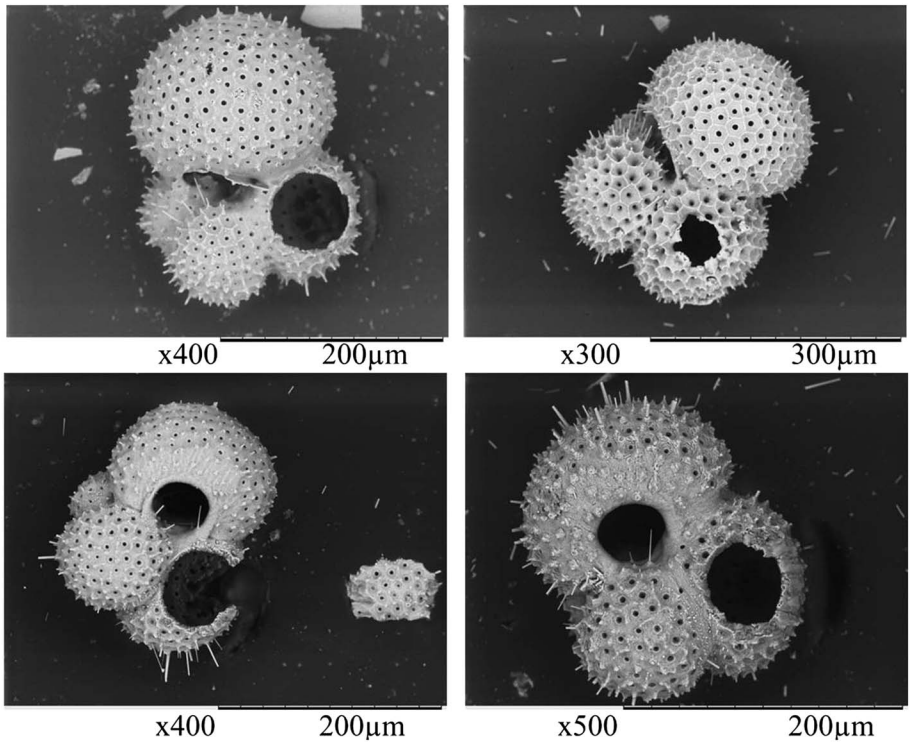

Figure 10. Specimens of (top row) *T. sacculifer* and (bottom row) *G. ruber* from surface water (plankton pump samples 4 and 7), showing an incipient cancellate surface with elevated spines bases.

the open ocean (Wit et al., 2010). Values measured are considerably lower compared to paleo Red Sea studies exhibiting inorganic overgrowth (Hoogakker et al., 2009). Still, average values are also similar to those observed for specimens of *T. sacculifer* that underwent GAM calcification (Nürnberg et al., 1996; Figure 13).

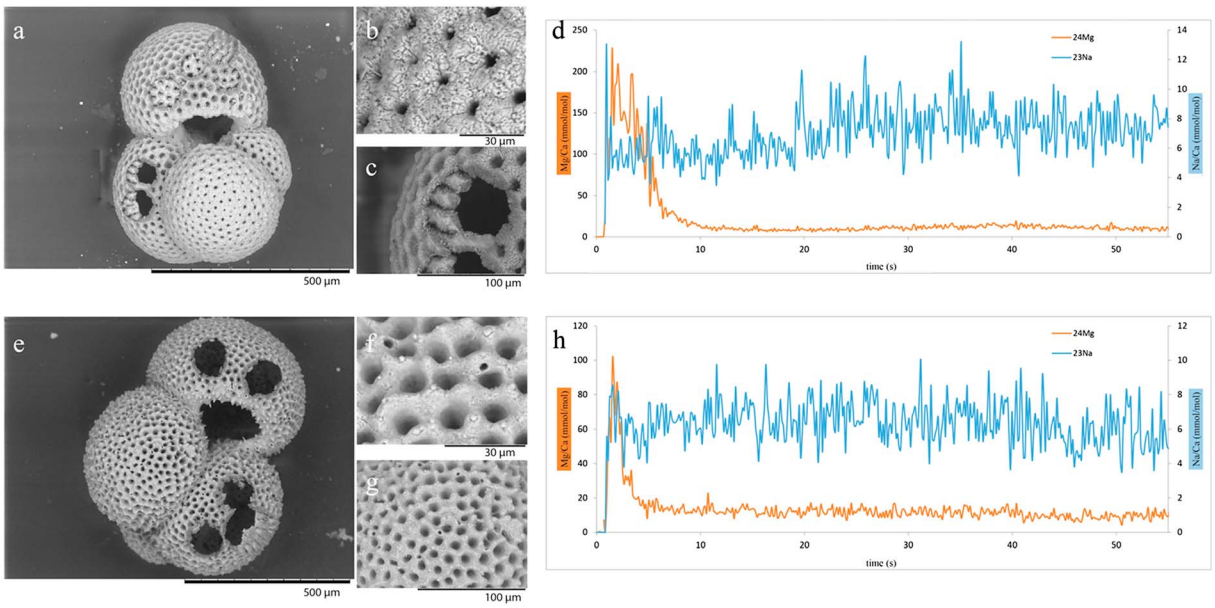

Figure 11. (a) Etched and thick gametogenesis (GAM) of a *T. sacculifer* from the northern Red Sea (core-top MC71, M5/2) with a (b) close-up of the surface structure, and (c) LA crater with a visible thick GAM calcite layer as indicated by (d) elevated Mg/Ca in the laser ablation profile. (e) Thick-walled *G. ruber* specimen from the same core-top with (f and g) GAM calcite and overgrown spine holes. Also slight signs of dissolution are visible and accompanying laser ablation profile showing a high Mg layer (GAM) at the outside of the shell.

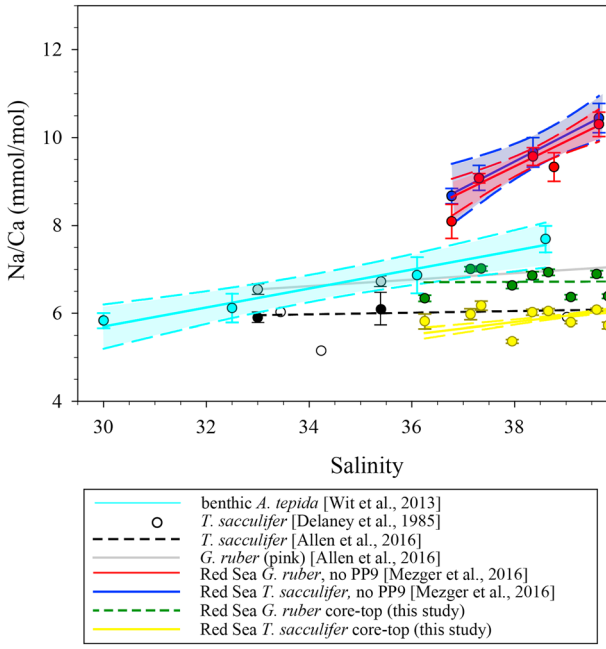

Figure 12. Core-top Na/Ca values versus sea surface salinity, compared to published relationships. Plankton pump 9 is excluded from the calibration, as described in Mezger et al. (2016).

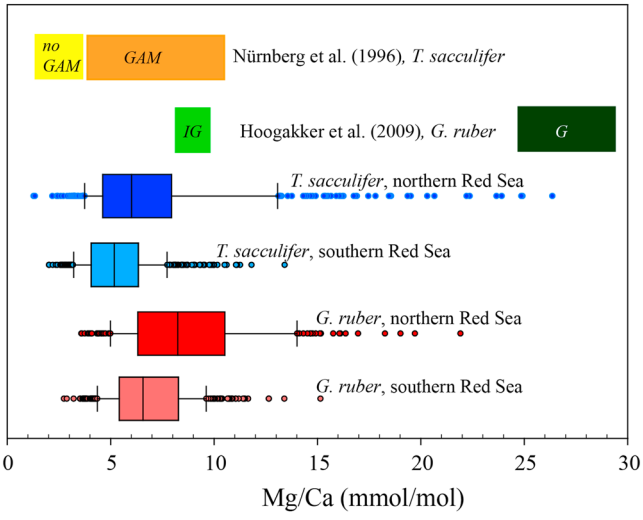

Figure 13. All core-top Mg/Ca values, compared to interglacial (IG) and glacial (G) Mg/Ca values for *G. ruber* specimens (whole-batch measurements FT-TRA-ICP-MS) including overgrowths (Hoogakker et al., 2009) and cultivated *T. sacculifer* specimens under different salinities and temperatures that underwent gametogenesis (GAM) and did not undergo gametogenesis (no-GAM; Nürnberg et al., 1996). The distinction between the northern (N) and southern (S) Red Sea is at 22.4°N and longitude of 37.5°E. Data from the Red Sea is based on single-chamber Mg/Ca (one dot is one laser ablation measurement), whereas variability in the other two data sets represents maximum and minimum values, resulting from interspecimen variability.

For foraminiferal specimens collected by plankton tows in the Red Sea (Figure 5) between 10 and 500 m of water depth, Na/Ca values are similar to those reported in previous studies (Allen et al., 2016; Delaney et al., 1985; Wit et al., 2013). However, Na/Ca and Mg/Ca in our specimens do not show a clear relationship to changes in salinity and/or temperature with depth. Whereas Na/Ca decreases with increasing water depth, Mg/Ca increases over the same depth interval (Figure 5). Given an approximate sinking speed between 198 and 838 m per day (*G. ruber*) and between 200 and 1,396 m per day (*T. sacculifer*) for postmortem planktonic foraminifera (Fok-Pun & Komar, 1983; Takahashi & Be, 1984; Van Sebille et al., 2015), only a very small fraction of specimens collected in each sample were sinking post mortem. Assuming that this has no appreciable effect on the results presented here, these trends in elemental compositions through the water column may reflect a combination of (1) ongoing calcification with depth-related environmental changes (e.g., salinity and temperature), (2) changes related to different life stages, and (3) chemical alteration of the shell within the water column.

4.1. Environmental Changes

4.1.1. Water Column Na/Ca and Mg/Ca

For both species, Na/Ca values decrease with increasing water depth within the upper 10–100 m of the water column and are consistent with the Na/Ca values observed in the surface water specimens (Mezger et al., 2016; Figure 12). Since it is known that Na/Ca in cultured benthic as well as cultured and field collected planktonic foraminiferal shells increases with salinity (Allen et al., 2016; Mezger et al., 2016; Wit et al., 2013) and salinity increases with depth in the Red Sea, it is unlikely that the observed decrease in Na/Ca is due to ongoing calcification with depth. In addition, temperature also decreases with depth, which would have an additional, albeit small, positive effect on Na/Ca (Allen et al., 2016).

The depth-resolved pattern in Mg/Ca is opposite to that in Na/Ca (Figure 5), as Mg/Ca increases with depth. Similar to Na/Ca, ongoing calcification with depth and the lower subsurface temperatures would result in lowering Mg/Ca rather than increasing it. Although salinity is known to affect Mg/Ca, the observed change of ~1 salinity unit (Figure 2) over the studied depth range is insufficient to fully explain the observed difference in Mg/Ca between living surface water specimens and plankton-tow specimens, as Mg-incorporation depends only to a limited extent on salinity compared to temperature (between 0.11 and 0.21 mmol/mol per salinity unit for an environmental relevant salinity range; Dueñas-Bohórquez et al., 2009; Gray et al., 2018; Hönisch et al., 2013; Kısakürek et al., 2008). Moreover, the difference in Na/Ca between *G. ruber* and *T. sacculifer* is not correlated with the difference in Mg/Ca between these species from the same depth interval.

These observations and the resulting opposing trends in Na/Ca and Mg/Ca compared to the seawater temperature and salinity profiles imply that continued calcification with depth cannot explain the observed trends. Consequently, the shell chemistry must have been altered by precipitation of chemically distinct calcite during changes in habitat and/or life-stage changes of the foraminifer.

4.1.2. Core Top Na/Ca and Mg/Ca

A small difference was observed between the deepest (300–500 m) water column samples and core-tops, with the core-top specimens being slightly lower in Na/Ca and slightly higher in Mg/Ca. A decrease in Na/Ca in fossil specimens has been observed before but was associated with aging over a time scale of several millions of years (Yoshimura et al., 2016). It was

observed that Na/Ca values decrease in a Quaternary core in the planktonic species *Globorotalia tumida*, which was attributed to ongoing leaching of Na from the crystal lattice. However, such an effect unlikely plays a role in foraminifera from core-tops as the time scale involved is much shorter.

Values reported for Mg/Ca here are also higher than those previously published for Mg/Ca in *G. ruber* and *T. sacculifer* species from culture studies and field calibrations (e.g., Allen et al., 2016; Anand et al., 2003; Kısakürek et al., 2008; Nürnberg et al., 1996). Since sea surface temperatures decrease toward the north of the Red Sea, Mg/Ca in specimens from the core-top samples show an apparent negative correlation to temperature and a positive correlation to salinity.

While *T. sacculifer* and *G. ruber* show similar Mg/Ca values at the sea surface (Mezger et al., 2016), both water column and core-top *T. sacculifer* show lower Mg/Ca values compared to *G. ruber*. Such an offset is consistent with results from several other studies (e.g., Anand et al., 2003; Nürnberg et al., 1996). In many culturing studies (e.g., Kısakürek et al., 2008) and field studies (e.g., Anand et al., 2003), it was found that Mg incorporation is positively correlated to temperature. Assuming continued calcification in the colder subsurface water, lower Mg/Ca values are expected for the plankton tow and core-top collected shells compared to specimens from surface waters (Allen et al., 2016; Anand et al., 2003; Kısakürek et al., 2008; Nürnberg et al., 1996). Even if salinity would have a much larger effect on Mg incorporation (Ferguson et al., 2008) than explained in section 4.1.1, the large changes in Mg/Ca with water depth observed here cannot be explained solely by continued calcification in deeper water, which is merely one salinity unit higher.

4.2. The Role of Spines on Shell Chemistry

One clue to explain the changes in Na/Ca of the shells comes from changes in shell preservation. The EPMA-based element distribution shows that Na is enriched in the spines and at the spine bases (Figures 4, 8, and 9). This is in contrast to the Mg/Ca distribution, showing a banding of the lamellar wall calcite similar to that observed earlier (e.g., Erez, 2003). The inhomogeneity in Na/Ca, related to the foraminiferal spines, offers an alternative explanation for the depth-related changes observed in Na/Ca. Loss of the spines during a foraminifer's life cycle would clearly result in an overall lowering of Na/Ca values (see mass balance calculation below). Foraminifera are known to shed their spines deeper in the water column before gamete release and also when under stress (e.g., Bé, 1980; Caron et al., 1990; Hemleben, 1975). Additionally, crystal growth rates for spines versus those for the shell calcite may explain differences in Na/Ca, as was shown in synthetically grown calcites (Busenberg & Plummer, 1985). As early stage foraminifera have a faster growth rate (Hemleben & Bijma, 1994), this could potentially also result in enhanced Na incorporation, whereas adult specimens with lower calcification rates might incorporate less Na. The combined effect of spine loss and decreasing growth rates with life stage and hence depth could therefore contribute to the observed decrease in Na/Ca values with depth. Since foraminifera do not secrete their shell at the same conditions throughout their life cycle, it remains, however, difficult to deconvolve such potential effects.

4.2.1. Spine-Related Na/Ca Change With Depth

Already the pioneering foraminiferal culture studies of (Bé, 1980; Caron et al., 1990; Hemleben, 1975) showed that foraminifera lose their spines at the end of their life cycle preceding gamete release or due to stress. For both species studied here spines protrude from the POS (primary organic sheet) through the entire chamber wall (Hemleben, 1975). During successive episodes of calcification, on the outer surface of the shell wall, calcite plaques build up around the spine bases, giving the surface a terraced structure (Bé, 1980; Hemleben, 1975; Spero, 1988; e.g., Figure 10). At the same time, a polygonal pattern of interpore ridges is deposited by the same process in *T. sacculifer* (Bé, 1980; e.g., Figure 10). In preparation for gametogenesis, these spines are possibly partially resorbed and subsequently shed by rhizopodial activity, resulting in the appearance of spine holes (Bé, 1980) similar to those observed here (Figure 11). Because of the high Na/Ca values of the spines, this results in shell Na/Ca values to decrease in fossil specimens as the relative contribution of the spines decreases. Often, only spine bases remain when specimens are deposited at the sediment. Confirming this hypothesis, all specimens collected from the surface water contain spines (Figure 4), whereas spines were no longer present for the specimens collected from the sediment surface (Figure 11).

For both species, lowest Na/Ca values are observed for the smallest size class in the water column (supporting information 1.1). Potentially, shell size could have an effect on the elemental ratios measured. For example, for Mg/Ca, Elderfield et al. (2002) found that with increasing shell size, Mg/Ca values increase. For Na/Ca, values increase with decreasing shell size in culture experiments with the benthic *A. tepida* (Wit

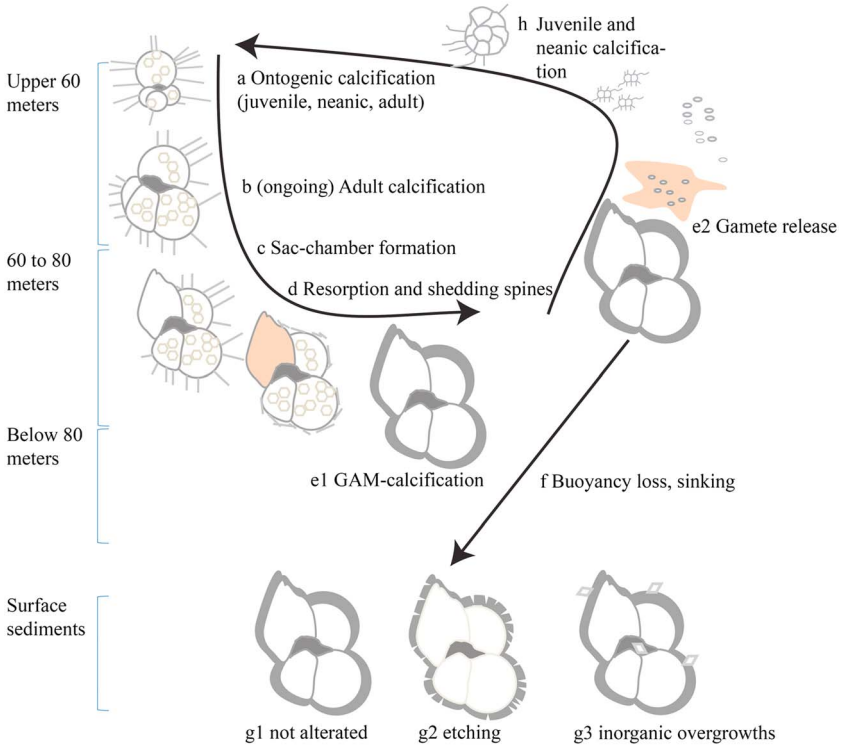

Figure 14. Morphology of *T. sacculifer* with depth and potential different life stages, based on Red Sea assemblage and depth studies of (Bé, 1980; Bijma & Hemleben, 1994; Brummer et al., 1986; Brown & Elderfield, 1996; Hemleben & Bijma, 1994; Brummer et al., 1987; Hoogakker et al., 2009). We assume the processes to be alike for *G. ruber*, but reproduction depths might be somewhat shallower.

et al., 2013) or chamber number (Mezger et al., 2016). However, it is argued that this relation is indirect, with salinity being the primary factor affecting shell size and thereby also Na incorporation (Mezger et al., 2016; Wit et al., 2013). In this study, no correlation is found between shell size and single-specimen Na/Ca for the core-top specimens, confirming that for spinose planktonic foraminifera, life stage (spines) rather than shell size determines the average Na/Ca measured. For *T. sacculifer,* highest core-top Mg/Ca values are observed for the largest specimens, albeit that this is also most probably associated with life stage (section 4.2.2) rather than shell size.

Measured spine LA-Q-ICP-MS Na/Ca values, confirmed by EPMA spine measurements, were up to 3 times higher compared to average foraminiferal shell Na/Ca values (Tables 3–6). A simple mass balance, based on measured spine Na/Ca values and the difference between core-top and surface water specimen Na/Ca values, shows that the difference between living and core-top specimens would require a relative spine contribution of 18.9% in *T. sacculifer* and 16.7% in *G. ruber*, respectively (Tables 5 and 6). These percentages represent the lower limit, as spines are often partly broken during sample collection and preparation. Bé (1980) and Erez and Honjo (1981) previously showed that GAM deposition potentially adds up to 28% or even 50% weight to the pre-GAM shell. Assuming that this calcite is possibly derived from resorbed spines (Bé, 1980), such a contribution of spines to the overall shell carbonate is not unrealistic. The loss of spines with depth hence likely explains the significant decrease of Na/Ca with depth in the upper 100 m of the water column, as reproduction in the Red Sea mostly occurs before 80 m depth (Bijma & Hemleben, 1994). Moreover, as spines have similar Mg/Ca-values as the shells (Tables 6), loss of spines unlikely affects the Mg/Ca signal.

Since the previously published Na/Ca to salinity relationships were based on chamber-specific spot analysis of the whole shell of specimens collected from the Red Sea surface water, a major part of this correlation must be due to spine chemistry. Such an (additional) impact of spine chemistry is in line with results obtained from a culturing study with the benthic foraminifer *A. tepida* (Wit et al., 2013), which is nonspinose, having much lower overall Na/Ca values and also a lower sensitivity toward salinity. Similarly, the cultured planktonic species used by Allen et al. (2016) likely lost part of their spines due to stress in a culture setting, explaining concentrations and sensitivity corresponding to the benthic species.

4.2.2. Spine Related Morphological Changes: Mg/Ca Change With Depth

As the Mg/Ca value of spines is similar compared to the shell Mg/Ca, higher Mg/Ca in the core-tops specimens cannot be explained by spine loss. However, also other morphological/terminal changes in many planktonic species may occur, potentially associated with spine loss (Figure 14).

After shedding of spines, ridged/terraced surface structures are replaced by a relatively smooth outer layer (GAM calcite) produced before gametogenesis (Bé, 1980; Bijma, Erez, et al., 1990; Brummer et al., 1987). Resorption of spines precedes precipitation of this GAM calcite (Bé, 1980), reducing the average Na/Ca. GAM calcite, as well as formation of another terminal feature like crust calcite, is known to change the elemental composition of the whole shell (Bijma, Faber, et al., 1990; Steinhardt et al., 2015). Because under natural conditions, deposition of GAM calcite often occurs in a deeper temperature and salinity environment compared to lamellar calcite precipitation; the impact of GAM and/or crust carbonate is difficult to quantify. Nürnberg et al. (1996) showed that *T. sacculifer* specimens that underwent GAM in culture under constant temperature conditions had much higher (up to 276% in GAM) Mg/Ca values compared to no-GAM specimens.

Values for Mg/Ca measured in planktonic foraminiferal shells collected in the northern Red Sea are similar to values reported by Hoogakker et al. (2009) for interglacial specimens of *T. sacculifer* collected down-core (Figure 13). With the exception of a few single tests, values are considerably lower than those of the glacial specimens, which according to Hoogakker et al. (2009) are related to the abnormally high salinities at those times causing secondary high Mg-rich overgrowths. Such inorganic overgrowths were not observed in SEM or EPMA images of the specimens studied here. van Raden et al. (2011) also found a layer of elevated (diagenetic) Mg/Ca values outside of the shell of *G. inflata* with laser ablation analysis, which was not visible in SEM images. We also observed a thin layer of high Mg/Ca on the outside of the shell of both species with laser ablation. The layer thickness seems to correspond to what morphologically seems GAM calcite adhered to the outside of the shell. The very high Mg/Ca values of this layer suggest that either the GAM calcite was precipitated strongly offset from pre-GAM carbonate or subsequently altered chemically without changing the morphology. The relatively high Mg/Ca of the GAM calcite makes this layer more prone to postmortem dissolution, causing the etched features on the outside of the shell (Figure 11).

For the Red Sea core-top specimens, a GAM layer is observed not only for *T. sacculifer* but also in *G. ruber* (Figure 11). The (increase in) average Mg/Ca and high variability in Mg/Ca for specimens $>$500 μm in *T. sacculifer* likely reflects differences in thickness of the GAM layer (Figure 11). After reproduction/gamete release (below 80 m depth), spinose foraminifera lose their buoyancy (Bijma & Hemleben, 1994). In the sediment, specimens containing a thick GAM layer are dominant over thin ontogenetic (only, or pre-GAM) shells (Bé, 1980). The relative contribution and thickness of GAM shells (Figure 11) and associated processes (spine loss) hence explains the increase in Mg/Ca with depth (increased contribution GAM shells), as well as the observed decrease in Na/Ca. Especially in the northern Red Sea core-tops, thick GAM shells are found (Figure 11), possibly explaining the observed extreme Mg/Ca values in the north and the apparent anti correlation with temperature.

4.2.3. Spine Ontogeny

Assuming that the loss or relative contribution of spines is responsible for observed differences in Na/Ca values between surface water, subsurface water column, and core-top specimens, this still does not explain the observed differences in slope for Na/Ca to salinity relationships (Allen et al., 2016; Mezger et al., 2016; Wit et al., 2013). Whereas the Na/Ca of specimens collected alive in surface waters show a high sensitivity to changes in salinity (Mezger et al., 2016), the response to salinity is more dampened in foraminiferal culture studies (Allen et al., 2016) and benthic species (Wit et al., 2013). Since we argue that spine chemistry may explain the observed difference between surface water and core-top specimens, this suggests that either spine Na/Ca or foraminiferal spine density (spines per chamber and/or spine length) increases with increasing salinity (Figure S5). Based on the measured Na/Ca values of the spines at a salinity of 39.6, this implies that for the Red Sea salinity range from 36 to 41 either *G. ruber* spine densities have to increase about three times (from 6.9 to 20.5%) and for *T. sacculifer* about 2 times (from 11.3 to 21.9%), or Na/Ca values increase approximately two times within the spines. These values have been calculated with two simple mass balances, assuming that the difference in Na/Ca between core-top and surface water calibrations for both species can be fully explained by an increase in spine density (assuming a constant spine Na/Ca) or spine Na/Ca values (assuming constant spine density). Although it is not possible to fully exclude a change in spine length, a shift in spine density high enough to explain the shift in Na/Ca values was not observed. Still, also the shell

chemistry itself will respond to salinity as observed for the benthic species *A. tepida* (Wit et al., 2013) and cultured planktonic ones (Allen et al., 2016), albeit with a much reduced sensitivity.

The relatively high Na/Ca in foraminiferal spines and spine bases may be associated with a difference in growth mechanism between spines and the rest of the shell. Assuming that the formation of foraminiferal spines is comparable to that of some other biogenic calcium carbonate structures (e.g., the spines of sea urchins), they consist of a single calcite crystal (Beniash et al., 1997; Hemleben, 1975; Rodriguez-Blanco et al., 2011). Such a single crystal-structure might result from an initial deposition of nanoparticles consisting of amorphous calcium carbonate that spontaneously form a single calcite crystal (Rodriguez-Blanco et al., 2011). Since the fluid-amorphous calcium carbonate transition is relatively fast compared to rates observed in nonbiogenic stepwise growth described from laboratory studies (Morse et al., 2007), the fractionation against, for example, Na, is less strong, and hence, the spines may have a higher Na/Ca than the rest of the shell. Also, this would imply a more direct, one to one, uptake of Na in spine carbonate in relation to salinity.

5. Conclusions

In this study, we tested the applicability of the foraminiferal Na/Ca-based salinity proxy by comparing the chemical composition of core-top and plankton tow collected planktonic foraminifera from the Red Sea to those living in surface waters. Results show that Na/Ca of both *G. ruber* and *T. sacculifer* decreases with increasing water depth, thereby dampening the initial Na/Ca to salinity signal. In contrast, Mg/Ca values increase for both species toward the seafloor. Laser-ablation-ICP-Q-MS measurements combined with EPMA show that for both species, Na is concentrated at the spines. Loss of spines in the water column provides a mechanistic explanation for the observed Na/Ca decrease with depth. Additionally, SEM pictures and LA profiles show that the deposition of GAM calcite—high in Mg, but with Na/Ca values similar to lamellar calcite—or (diagenetic) recrystallization of GAM calcite explains the increasing Mg/Ca values. Na/Ca values of the core-top specimens coincide with the earlier established correlation with salinity for benthic and planktonic foraminifera from controlled growth experiments. This study revealed the unexpected role of spine calcite on foraminiferal Na/Ca and found that Mg/Ca is elevated beyond known salinity and temperature calibrations, requiring an additional process enriching Mg in shells. The origin of the Na/Ca signal is better understood now but still requires more research to serve as a robust proxy for salinity.

Acknowledgments
This research is funded by the NIOZ-Royal Netherlands Institute for Sea Research and supported by the Gravitation grant NESSC from the Dutch Ministry of Education, Culture, and Science. We thank W. Boer (NIOZ) and T. Bouten (Utrecht University) for their analytical assistance. We are also grateful to all technical staff onboard of RV *Pelagia* cruise 64PE158 and the other cruises. This research did not receive any specific grant from funding agencies in the public, commercial, or not-for-profit sectors.

References

Allen, K. A., Hönisch, B., Eggins, S. M., Haynes, L. L., Rosenthal, Y., & Yu, J. (2016). Trace element proxies for surface ocean conditions: A synthesis of culture calibrations with planktic foraminifera. *Geochimica et Cosmochimica Acta*, *193*, 197–221. https://doi.org/10.1016/j.gca.2016.08.015

Anand, P., Elderfield, H., & Conte, M. H. (2003). Calibration of Mg/Ca thermometry in planktonic foraminifera from a sediment trap time series. *Paleoceanography*, *18*(2), 1050. https://doi.org/10.1029/2002PA000846

Antonov, J., Seidov, D., Boyer, T., Locarnini, R., Mishonov, A., Garcia, H., et al. (2010). In S. Levitus (Ed.), *World Ocean Atlas 2009, vol. 2: Salinity*, NOAA Atlas NESDIS, (Vol. *69*, p. 184). Washington, D.C: Government Printing Office.

Barker, S., Greaves, M., & Elderfield, H. (2003). A study of cleaning procedures used for foraminiferal Mg/Ca paleothermometry. *Geochemistry, Geophysics, Geosystems*, *4*(9), 8407. https://doi.org/10.1029/2003GC000559

Bé, A. W. H. (1980). Gametogenic calcification in a spinose planktonic foraminifer, Globigerinoides sacculifer (Brady). *Marine Micropaleontology*, *5*, 283–310. https://doi.org/10.1016/0377-8398(80)90014-6

Beniash, E., Aizenberg, J., Addadi, L., & Weiner, S. (1997). Amorphous calcium carbonate transforms into calcite during sea urchin larval spicule growth. *Proceedings of the Royal Society of London B: Biological sciences*, *264*(1380), 461–465. https://doi.org/10.1098/rspb.1997.0066

Bijma, J., Erez, J., & Hemleben, C. (1990). Lunar and semi-lunar reproductive cycles in some spinose planktonic foraminifers. *Journal of Foraminiferal Research*, *20*(2), 117–127. https://doi.org/10.2113/gsjfr.20.2.117

Bijma, J., Faber, W. W., & Hemleben, C. (1990). Temperature and salinity limits for growth and survival of some planktonic foraminifers in laboratory cultures. *Journal of Foraminiferal Research*, *20*(2), 95–116. https://doi.org/10.2113/gsjfr.20.2.95

Bijma, J., & Hemleben, C. (1994). Population dynamics of the planktic foraminifer Globigerinoides sacculifer (Brady) from the central Red Sea. *Deep Sea Research Part I: Oceanographic Research Papers*, *41*(3), 485–510. https://doi.org/10.1016/0967-0637(94)90092-2

Brown, S. J., & Elderfield, H. (1996). Variations in Mg/Ca and Sr/Ca ratios of planktonic foraminifera caused by postdepositional dissolution: Evidence of shallow Mg-dependent dissolution. *Paleoceanography*, *11*, 543–551. https://doi.org/10.1029/96PA01491

Brummer, G.-J. A., Hemleben, C., & Spindler, M. (1986). Planktonic foraminiferal ontogeny and new perspectives for micropalaeontology. *Nature*, *319*(6048), 50–52. https://doi.org/10.1038/319050a0

Brummer, G.-J. A., Hemleben, C., & Spindler, M. (1987). Ontogeny of extant spinose planktonic foraminifera (Globigerinidae): A concept exemplified by Globigerinoides sacculifer (Brady) and G. Ruber (D'Orbigny). *Marine Micropaleontology*, *12*, 357–381. https://doi.org/10.1016/0377-8398(87)90028-4

Busenberg, E., & Plummer, L. N. (1985). Kinetic and thermodynamic factors controlling the distribution of SO32− and Na+ in calcites and selected aragonites. *Geochimica et Cosmochimica Acta*, *49*(3), 713–725. https://doi.org/10.1016/0016-7037(85)90166-8

Caron, D. A., Anderson, O. R., Lindsey, J. L., Faber, W. W., & Lim, E. L. (1990). Effects of gametogenesis on test structure and dissolution of some spinose planktonic foraminifera and implications for test preservation. *Marine Micropaleontology*, *16*(1–2), 93–116. https://doi.org/10.1016/0377-8398(90)90031-G

De Nooijer, L. J., Reichart, G.-J., Dueñas-Bohórquez, A., Wolthers, M., Ernst, S., Mason, P., et al. (2007). Copper incorporation in foraminiferal calcite: Results from culturing experiments. *Biogeosciences Discussions*, *4*(4), 493–504. https://doi.org/10.5194/bg-4-493-2007

Delaney, M. L., Bé, A. W. H., & Boyle, E. A. (1985). Li, Sr, Mg, and Na in foraminiferal calcite shells from laboratory culture, sediment traps, and sediment cores. *Geochimica et Cosmochimica Acta*, *49*(6), 1327–1341. https://doi.org/10.1016/0016-7037(85)90284-4

Dueñas-Bohórquez, A., Da Rocha, R. E., Kuroyanagi, A., Bijma, J., & Reichart, G. J. (2009). Effect of salinity and seawater calcite saturation state on Mg and Sr incorporation in cultured planktonic foraminifera. *Marine Micropaleontology*, *73*(3-4), 178–189. https://doi.org/10.1016/j.marmicro.2009.09.002

Dueñas-Bohórquez, A., Da Rocha, R. E., Kuroyanagi, A., Bijma, J., & Reichart, G. J. (2011). Interindividual variability and ontogenetic effects on Mg and Sr incorporation in the planktonic foraminifer Globigerinoides sacculifer. *Geochimica et Cosmochimica Acta*, *75*(2), 520–532. https://doi.org/10.1016/j.gca.2010.10.006

Elderfield, H., & Ganssen, G. (2000). Past temperature and d18O of surface ocean waters inferred from foraminiferal Mg/Ca ratios. *Nature*, *405*(6785), 442–445. https://doi.org/10.1038/35013033

Elderfield, H., Vautravers, M., & Cooper, M. (2002). The relationship between shell size and Mg/Ca, Sr/Ca, δ18O, and δ13C of species of planktonic foraminifera. *Geochemistry, Geophysics, Geosystems*, *3*(8), 1052. https://doi.org/10.1029/2001GC000194

Erez, J. (2003). The source of ions for biomineralization in foraminifera and their implications for paleoceanographic proxies. *Reviews in Mineralogy and Geochemistry*, *54*(1), 115–149. https://doi.org/10.2113/0540115

Erez, J., & Honjo, S. (1981). Comparison of isotopic composition of planktonic foraminifera in plankton tows, sediment traps and sediments. *Palaeogeography, Palaeoclimatology, Palaeoecology*, *33*(1–3), 129–156. https://doi.org/10.1016/0031-0182(81)90035-3

Evans, D., Erez, J., Oron, S., & Müller, W. (2015). Mg/Ca-temperature and seawater-test chemistry relationships in the shallow-dwelling large benthic foraminifera Operculina ammonoides. *Geochimica et Cosmochimica Acta*, *148*, 325–342. https://doi.org/10.1016/j.gca.2014.09.039

Fallet, U., Boer, W., van Assen, C., Greaves, M., & Brummer, G. J. A. (2009). A novel application of wet oxidation to retrieve carbonates from large organic-rich samples for ocean-climate research. *Geochemistry, Geophysics, Geosystems*, *10*, Q08004. https://doi.org/10.1029/2009GC002573

Ferguson, J., Henderson, G., Kucera, M., & Rickaby, R. (2008). Systematic change of foraminiferal Mg/Ca ratios across a strong salinity gradient. *Earth and Planetary Science Letters*, *265*(1-2), 153–166. https://doi.org/10.1016/j.epsl.2007.10.011

Fietzke, J., & Frische, M. (2016). Experimental evaluation of elemental behavior during LA-ICP-MS: Influences of plasma conditions and limits of plasma robustness. *Journal of Analytical Atomic Spectrometry*, *31*(1), 234–244. https://doi.org/10.1039/C5JA00253B

Fok-Pun, L., & Komar, P. D. (Producer). (1983). Settling velocities of planktonic-foraminifer: Density variations and shape effects. *Journal of Foraminiferal Research, 13*(1), 60-68.

Geerken, E., de Nooijer, L. J., van Dijk, I., & Reichart, G. J. (2018). Impact of salinity on element incorporation in two benthic foraminiferal species with contrasting magnesium contents. *Biogeosciences*, *15*(7), 2205–2218. https://doi.org/10.5194/bg-15-2205-2018

Gordon, C., Carr, R., & Larson, R. (1970). The influence of environmental factors on the sodium and manganese content of barnacle shells. *Limnology and Oceanography*, *15*(3), 461–466. https://doi.org/10.4319/lo.1970.15.3.0461

Gray, W. R., Weldeab, S., Lea, D. W., Rosenthal, Y., Gruber, N., Donner, B., et al. (2018). The effects of temperature, salinity, and the carbonate system on Mg/Ca in Globigerinoides ruber (white): A global sediment trap calibration. *Earth and Planetary Science Letters*, *482*, 607–620. https://doi.org/10.1016/j.epsl.2017.11.026

Hathorne, E. C., James, R. H., Savage, P., & Alard, O. (2008). Physical and chemical characteristics of particles produced by laser ablation of biogenic calcium carbonate. *Journal of Analytical Atomic Spectrometry*, *23*(2), 240–243. https://doi.org/10.1039/B706727E

Hemleben, C. (1975). Spine and pustule relationships in some recent planktonic foraminifers. *Micropaleontology*, *21*(3), 334–341. https://doi.org/10.2307/1485199

Hemleben, C., & Bijma, J. (1994). Foraminiferal population dynamics and stable carbon isotopes. In *Carbon cycling in the glacial ocean: Constraints on the ocean's role in global change*, (pp. 145–166). Berlin, Heidelberg: Springer.

Hönisch, B., Allen, K. A., Lea, D. W., Spero, H. J., Eggins, S. M., Arbuszewski, J., et al. (2013). The influence of salinity on Mg/Ca in planktic foraminifers—Evidence from cultures, core-top sediments and complementary δ18O. *Geochimica et Cosmochimica Acta*, *121*, 196–213. https://doi.org/10.1016/j.gca.2013.07.028

Hönisch, B., Allen, K. A., Russell, A., Eggins, S. M., Bijma, J., Spero, H. J., et al. (2011). Planktic foraminifers as recorders of seawater Ba/Ca. *Marine Micropaleontology*, *79*(1-2), 52–57. https://doi.org/10.1016/j.marmicro.2011.01.003

Hoogakker, B. A. A., Klinkhammer, G. P., Elderfield, H., Rohling, E. J., & Hayward, C. (2009). Mg/Ca paleothermometry in high salinity environments. *Earth and Planetary Science Letters*, *284*(3-4), 583–589. https://doi.org/10.1016/j.epsl.2009.05.027

Ishikawa, M., & Ichikuni, M. (1984). Uptake of sodium and potassium by calcite. *Chemical Geology*, *42*(1-4), 137–146. https://doi.org/10.1016/0009-2541(84)90010-X

Jochum, K. P., Weis, U., Stoll, B., Kuzmin, D., Yang, Q., Raczek, I., et al. (2011). Determination of reference values for NIST SRM 610–617 glasses following ISO guidelines. *Geostandards and Geoanalytical Research*, *35*(4), 397–429. https://doi.org/10.1111/j.1751-908X.2011.00120.x

Kısakürek, B., Eisenhauer, A., Böhm, F., Garbe-Schönberg, D., & Erez, J. (2008). Controls on shell Mg/Ca and Sr/Ca in cultured planktonic foraminiferan, *Globigerinoides ruber* (white). *Earth and Planetary Science Letters*, *273*(260–269). https://doi.org/10.1016/j.epsl.2008.06.026

Kitano, Y., Okumura, M., & Idogaki, M. (1975). Incorporation of sodium, chloride and sulfate with calcium carbonate. *Geochemical Journal*, *9*(2), 75–84. https://doi.org/10.2343/geochemj.9.75

Lea, D. W., & Boyle, E. A. (1991). Barium in planktonic foraminifera. *Geochimica et Cosmochimica Acta*, *55*(11), 3321–3331. https://doi.org/10.1016/0016-7037(91)90491-M

Lea, D. W., Mashiotta, T. A., & Spero, H. J. (1999). Controls on magnesium and strontium uptake in planktonic foraminifera determined by live culturing. *Geochimica et Cosmochimica Acta*, *63*(16), 2369–2379. https://doi.org/10.1016/S0016-7037(99)00197-0

Locarnini, R., Mishonov, A., Antonov, J., Boyer, T., Garcia, H., Baranova, O., et al. (2010). In S. Levitus (Ed.), *World Ocean Atlas 2009, vol. 1, temperature*, (p. 184). Washington, DC: *US Gov. Print. Off.*

Mezger, E. M., Nooijer, L. J., Boer, W., Brummer, G. J. A., & Reichart, G. J. (2016). Salinity controls on Na incorporation in Red Sea planktonic foraminifera. *Paleoceanography*, *31*, 1562–1582. https://doi.org/10.1002/2016PA003052

Morse, J. W., Arvidson, R. S., & Lüttge, A. (2007). Calcium carbonate formation and dissolution. *Chemical Reviews*, *107*(2), 342–381. https://doi.org/10.1021/cr050358j

Nürnberg, D., Bijma, J., & Hemleben, C. (1996). Assessing the reliability of magnesium in foraminiferal calcite as a proxy for water mass temperatures. *Geochimica et Cosmochimica Acta*, *60*(5), 803–814. https://doi.org/10.1016/0016-7037(95)00446-7

Prahl, F., & Wakeham, S. (1987). Calibration of unsaturation patterns in long-chain ketone compositions for palaeotemperature assessment. *Nature*, *330*(6146), 367–369. https://doi.org/10.1038/330367a0

Rodriguez-Blanco, J. D., Shaw, S., & Benning, L. G. (2011). The kinetics and mechanisms of amorphous calcium carbonate (ACC) crystallization to calcite, via vaterite. *Nanoscale*, *3*(1), 265–271. https://doi.org/10.1039/C0NR00589D

Rohling, E. J. (1994). Glacial conditions in the Red Sea. *Paleoceanography*, *9*, 653–660. https://doi.org/10.1029/94PA01648

Rohling, E. J. (2007). Progress in paleosalinity: Overview and presentation of a new approach. *Paleoceanography*, *22*, PA3215. https://doi.org/10.1029/2007PA001437

Rohling, E. J., & Bigg, G. R. (1998). Paleosalinity and d180: A critical assessment. *Journal of Geophysical Research*, *103*, 1307–1318. https://doi.org/10.1029/97JC01047

Rucker, J. B., & Valentine, J. W. (1961). Salinity response of trace element concentration in *Crassostrea virginica*. *Nature*, *190*(4781), 1099–1100. https://doi.org/10.1038/1901099a0

Sadekov, A. Y., Eggins, S. M., & De Deckker, P. (2005). Characterization of Mg/Ca distributions in planktonic foraminifera species by electron microprobe mapping. *Geochemistry, Geophysics, Geosystems*, *6*, Q12P06. https://doi.org/10.1029/2005GC000973

Schouten, S., Hopmans, E. C., Schefuß, E., & Sinninghe Damste, J. S. (2002). Distributional variations in marine crenarchaeotal membrane lipids: A new tool for reconstructing ancient sea water temperatures? *Earth and Planetary Science Letters*, *204*(1-2), 265–274. https://doi.org/10.1016/S0012-821X(02)00979-2

Schouten, S., Ossebaar, J., Schreiber, K., Kienhuis, M., Langer, G., Benthien, A., et al. (2006). The effect of temperature, salinity and growth rate on the stable hydrogen isotopic composition of long chain alkenones produced by Emiliania huxleyi and Gephyrocapsa oceanica. *Biogeosciences*, *3*(1), 113–119. https://doi.org/10.5194/bg-3-113-2006

Segev, E., & Erez, J. (2006). Effect of Mg/Ca ratio in seawater on shell composition in shallow benthic foraminifera. *Geochemistry, Geophysics, Geosystems*, *7*, Q02P09. https://doi.org/10.1029/2005GC000969

Sicha, M., Trommer, G., Schulz, H., Hemleben, C., & Kucera, M. (2009). Factors controlling the distribution of planktonic foraminifera in the Red Sea and implications for the development of transfer functions. *Marine Micropaleontology*, *72*(3-4), 146–156. https://doi.org/10.1016/j.marmicro.2009.04.002

Spero, H. (1988). Ultrastructural examination of chamber morphogenesis and biomineralization in the planktonic foraminifer Orbulina universa. *Marine Biology*, *99*(1), 9–20. https://doi.org/10.1007/BF00644972

Spezzaferri, S., Kucera, M., Pearson, P. N., Wade, B. S., Rappo, S., Poole, C. R., et al. (2015). Fossil and genetic evidence for the polyphyletic nature of the planktonic foraminifera Globigerinoides, and description of the new genus Trilobatus. *PLoS One*, *10*(5), e0128108. https://doi.org/10.1371/journal.pone.0128108

Steinhardt, J., de Nooijer, L. J., Brummer, G. J., & Reichart, G. J. (2015). Profiling planktonic foraminiferal crust formation. *Geochemistry, Geophysics, Geosystems*, *16*, 2409–2430. https://doi.org/10.1002/2015GC005752

Takahashi, K., & Be, A. W. H. (1984). Planktonic foraminifera: Factors controlling sinking speeds. *Deep Sea Research Part A. Oceanographic Research Papers*, *31*(12), 1477–1500. https://doi.org/10.1016/0198-0149(84)90083-9

van Dijk, I., de Nooijer, L. J., & Reichart, G.-J. (2017). Trends in element incorporation in hyaline and porcelaneous foraminifera as a function of pCO 2. *Biogeosciences*, *14*(3), 497–510. https://doi.org/10.5194/bg-14-497-2017

van Raden, U. J., Groeneveld, J., Raitzsch, M., & Kucera, M. (2011). Mg/Ca in the planktonic foraminifera Globorotalia inflata and Globigerinoides bulloides from Western Mediterranean plankton tow and core top samples. *Marine Micropaleontology*, *78*(3–4), 101–112. https://doi.org/10.1016/j.marmicro.2010.11.002

Van Sebille, E., Scussolini, P., Durgadoo, J. V., Peeters, F. J., Biastoch, A., Weijer, W., et al. (2015). Ocean currents generate large footprints in marine palaeoclimate proxies. *Nature Communications*, *6*(1), 6521. https://doi.org/10.1038/ncomms7521

Vasiliev, I., Mezger, E. M., Lugli, S., Reichart, G.-J., Manzi, V., & Roveri, M. (2017). How dry was the Mediterranean during the Messinian salinity crisis? *Palaeogeography, Palaeoclimatology, Palaeoecology*, *471*, 120–133. https://doi.org/10.1016/j.palaeo.2017.01.032

Wilson, S., Koenig, A., & Orklid, R. (2008). Development of microanalytical reference material (MACS-3) for LA-ICP-MS analysis of carbonate samples. *Geochimica et Cosmochimica Acta Supplement*, *72*, A1025.

Wit, J. C., De Nooijer, L., Wolthers, M., & Reichart, G.-J. (2013). A novel salinity proxy based on Na incorporation into foraminiferal calcite. *Biogeosciences*, *10*(10), 6375–6387. https://doi.org/10.5194/bg-10-6375-2013

Wit, J. C., Reichart, G.-J., Jung, J. A., & Kroon, A. (2010). Approaches to unravel seasonality in sea surface temperatures using paired single-specimen foraminiferal d18O and Mg/Ca analyses. *Paleoceanography*, *25*, Pa4220. https://doi.org/10.1029/2009PA001857

Yoshimura, T., Tamenori, Y., Suzuki, A., Kawahata, H., Iwasaki, N., Hasegawa, H., et al. (2016). Altervalent substitution of sodium for calcium in biogenic calcite and aragonite. *Geochimica et Cosmochimica Acta*, *202*, 21–38. https://doi.org/10.1016/j.gca.2016.12.003

Zachos, J., Pagani, M., Sloan, L., Thomas, E., & Billups, K. (2001). Trends, rhythms, and aberrations in global climate 65 Ma to present. *Science*, *292*(5517), 686–693. https://doi.org/10.1126/science.1059412

Zahn, R., & Mix, A. C. (1991). Benthic foraminiferal δ18O in the ocean's temperature-salinity-density field: Constraints on Ice Age thermohaline circulation. *Paleoceanography*, *6*, 1–20. https://doi.org/10.1029/90PA01882